Cell

Article

Population-scale tissue transcriptomics maps long non-coding RNAs to complex disease

Graphical abstract

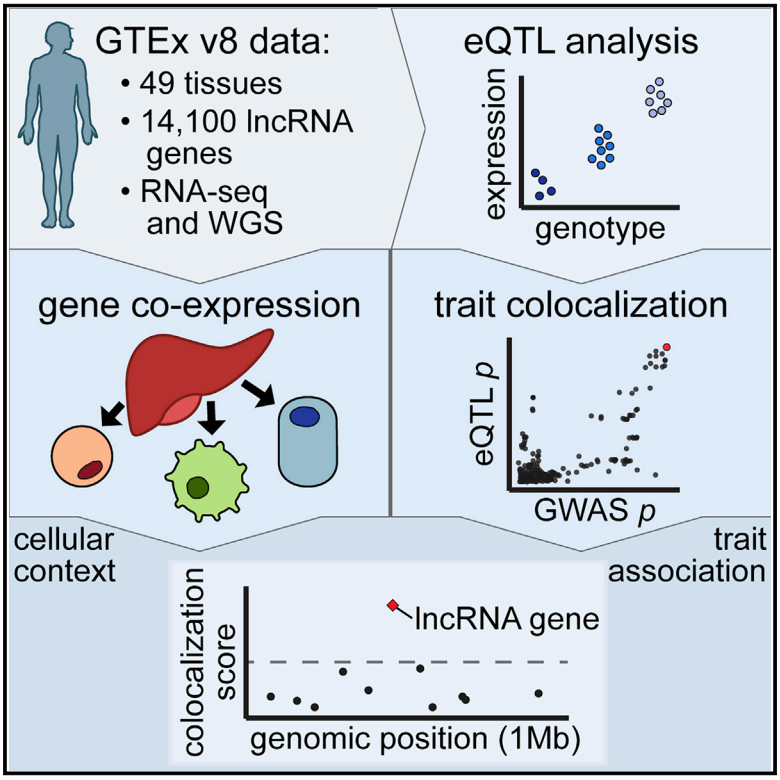

Authors

Olivia M. de Goede, Daniel C. Nachun, Nicole M. Ferraro, ..., Thomas Quertermous, Karla Kirkegaard, Stephen B. Montgomery

Correspondence

odegoede@stanford.edu (O.M.d.G.), smontgom@stanford.edu (S.B.M.)

In brief

A systematic analysis of NIH Genotype Tissue Expression (GTEx) project data provides insights into lncRNA expression patterns and functions, explores the impact of genetic variation on lncRNAs, and connects lncRNAs to complex traits and human disease.

Highlights

- 29% of lncRNA genes with eQTLs show tissue-specific genetic regulation
- Co-expression networks and single-cell data provide annotations for 94% of lncRNAs
- Rare variants near lncRNA expression outliers impact complex traits, like BMI
- We identify 800 lncRNA-trait relationships not explained by protein-coding genes

de Goede et al., 2021, Cell *184*, 2633–2648
May 13, 2021
https://doi.org/10.1016/j.cell.2021.03.050

CellPress

Cell

CellPress

Article

Population-scale tissue transcriptomics maps long non-coding RNAs to complex disease

Olivia M. de Goede,[1,*] Daniel C. Nachun,[2] Nicole M. Ferraro,[3] Michael J. Gloudemans,[3] Abhiram S. Rao,[4] Craig Smail,[3,5] Tiffany Y. Eulalio,[3] François Aguet,[6] Bernard Ng,[7,8] Jishu Xu,[9] Alvaro N. Barbeira,[10] Stephane E. Castel,[11,12] Sarah Kim-Hellmuth,[11,12,13] YoSon Park,[14] Alexandra J. Scott,[15] Benjamin J. Strober,[16] GTEx Consortium, Christopher D. Brown,[17] Xiaoquan Wen,[18] Ira M. Hall,[19] Alexis Battle,[16,20] Tuuli Lappalainen,[11,12] Hae Kyung Im,[10] Kristin G. Ardlie,[6] Sara Mostafavi,[21] Thomas Quertermous,[22] Karla Kirkegaard,[1,23] and Stephen B. Montgomery[1,2,24,*]

[1]Department of Genetics, Stanford University, Stanford, CA 94305, USA
[2]Department of Pathology, Stanford University, Stanford, CA 94305, USA
[3]Biomedical Informatics Training Program, Stanford University, Stanford, CA 94305, USA
[4]Department of Bioengineering, Stanford University, Stanford, CA 94305, USA
[5]Genomic Medicine Center, Children's Mercy Research Institute, Kansas City, MO 64108, USA
[6]The Broad Institute of MIT and Harvard, Cambridge, MA 02142, USA
[7]Department of Statistics, University of British Columbia, Vancouver, BC V6T 1Z4, Canada
[8]Centre for Molecular Medicine and Therapeutics, Vancouver, BC V5Z 4H4, Canada
[9]Rush Alzheimer's Disease Center, Rush University, Chicago, Illinois 60612, USA
[10]Section of Genetic Medicine, Department of Medicine, The University of Chicago, Chicago, IL 60637, USA
[11]New York Genome Center, New York, NY 10013, USA
[12]Department of Systems Biology, Columbia University, New York, NY 10032, USA
[13]Department of Pediatrics, Dr. von Hauner Children's Hospital, University Hospital LMU Munich, Munich 80337, Germany
[14]Department of Systems Pharmacology and Translational Therapeutics, University of Pennsylvania, Perelman School of Medicine, Philadelphia, PA 19104, USA
[15]McDonnell Genome Institute, Washington University School of Medicine, St. Louis, MO 63108, USA
[16]Department of Biomedical Engineering, Johns Hopkins University, Baltimore, MD 21218, USA
[17]Department of Genetics, University of Pennsylvania, Perelman School of Medicine, Philadelphia, PA 19104, USA
[18]Department of Biostatistics, University of Michigan, Ann Arbor, MI 48109, USA
[19]Department of Genetics, Yale University School of Medicine, New Haven, CT 06510, USA
[20]Department of Computer Science, Johns Hopkins University, Baltimore, MD 21218, USA
[21]Paul G. Allen School of Computer Science and Engineering, University of Washington, Seattle, WA 98195, USA
[22]Division of Cardiovascular Medicine and Cardiovascular Institute, Stanford University, Stanford, CA 94305, USA
[23]Department of Microbiology and Immunology, Stanford University, Stanford, CA 94305, USA
[24]Lead contact
*Correspondence: odegoede@stanford.edu (O.M.d.G.), smontgom@stanford.edu (S.B.M.)
https://doi.org/10.1016/j.cell.2021.03.050

SUMMARY

Long non-coding RNA (lncRNA) genes have well-established and important impacts on molecular and cellular functions. However, among the thousands of lncRNA genes, it is still a major challenge to identify the subset with disease or trait relevance. To systematically characterize these lncRNA genes, we used Genotype Tissue Expression (GTEx) project v8 genetic and multi-tissue transcriptomic data to profile the expression, genetic regulation, cellular contexts, and trait associations of 14,100 lncRNA genes across 49 tissues for 101 distinct complex genetic traits. Using these approaches, we identified 1,432 lncRNA gene-trait associations, 800 of which were not explained by stronger effects of neighboring protein-coding genes. This included associations between lncRNA quantitative trait loci and inflammatory bowel disease, type 1 and type 2 diabetes, and coronary artery disease, as well as rare variant associations to body mass index.

INTRODUCTION

Long non-coding RNA (lncRNA) genes are a prevalent and heterogeneous group of RNA molecules that lack protein-coding potential. They vary in their epigenetic marks and in splicing and transcript structure (Amin et al., 2015; Hon et al., 2017; Melé et al., 2017; Quinn and Chang, 2016), and they differ from protein-coding genes due to their lower expression, increased tissue specificity, and greater variability in expression across individuals (Cabili et al., 2011; Djebali et al., 2012; Hon et al., 2017; Kornienko et al., 2016; Melé et al., 2015). Despite these differences, many lncRNA genes have important roles in gene

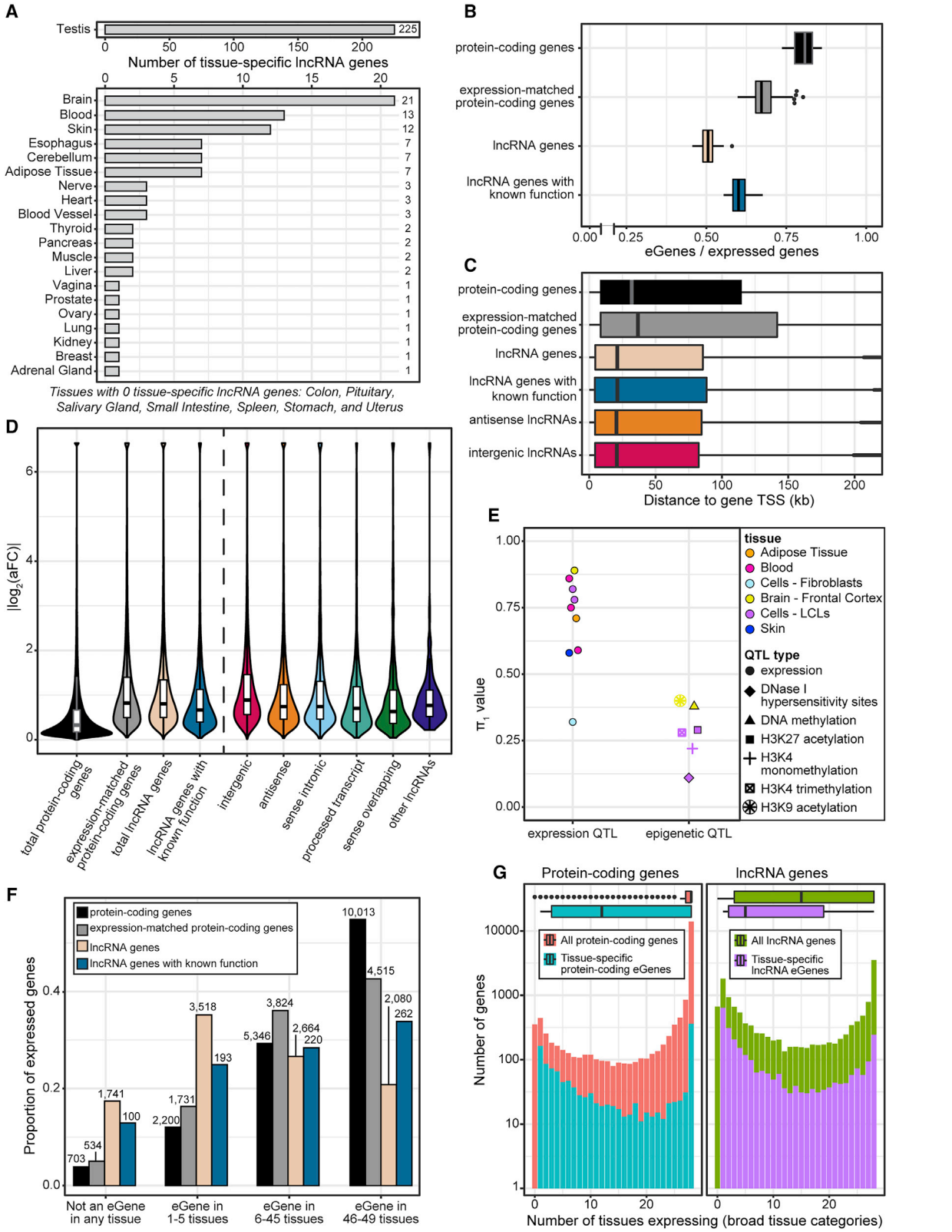

(legend on next page)

regulation, from epigenetic reprogramming to post-transcriptional regulation (Quinn and Chang, 2016; Wang and Chang, 2011). However, only a few of these lncRNAs have been connected to trait and disease outcomes, such as *HOTAIR* in cancer, *BACE1-AS* in Alzheimer's disease, and *PRNCR1* and *PCGEM1* in prostate cancer (Faghihi et al., 2008; Gupta et al., 2010; Yang et al., 2013). Although the number of annotated lncRNA genes is increasing with more sensitive transcriptomic profiling in a wider range of contexts and across more individuals (Djebali et al., 2012; Hon et al., 2017; Iyer et al., 2015; Jiang et al., 2019), it remains a significant challenge to identify those lncRNAs with important functional consequences.

In this study, we used data from the Genotype Tissue Expression (GTEx) project v8 to profile genetic regulation of lncRNA genes across 49 human tissues. We combine multiple approaches, including expression quantitative trait locus (eQTL) analysis, gene expression outlier analysis, co-expression networks, and genome-wide association study (GWAS)-QTL colocalization analysis, to identify putative functional lncRNA genes, define their cellular contexts, and systematically assess their relevance to diverse human traits. Together, this work increases the number of lncRNA genes with regulatory connections to human disease.

RESULTS

Expression of lncRNA genes across multiple tissue transcriptomes

Across tissue transcriptomes, we observed expression of the majority (95%) of the 14,100 previously annotated lncRNA genes in at least one tissue (Figures S1A and S1B). Among these, 96% of our curated list of 954 lncRNA genes with previous established functions were expressed in at least one tissue (Table S1; STAR Methods). We further stratified lncRNA genes into antisense and intergenic, as these two types make up the majority of lncRNA genes (at 5,220 and 7,433 genes, respectively), and observed expression of 96.5% and 94% of them, respectively.

There is previous evidence of the tissue specificity of lncRNA gene expression, especially for intergenic lncRNA genes, which is also observed in GTEx data (Figure S1C) (Cabili et al., 2011; Djebali et al., 2012; Hon et al., 2017; Jiang et al., 2019; Melé et al., 2015). The tissue specificity of lncRNA gene expression has been attributed to tissue-specific functions, spurious transcription, and effects of thresholding on detecting lowly expressed genes. To extend these analyses and mitigate overestimates of tissue specificity due to thresholding effects, we used an approach inspired by microarrays to identify tissue-specific lncRNA genes. For each of the 14,100 lncRNA genes, we defined a length-matched, non-genic region as close to the gene as possible; lncRNA genes were then called expressed in a given sample if the read count for the gene was significantly greater than for the matched non-genic region (Figure S1D; Table S1; STAR Methods). This resulted in lncRNA genes being detected in more tissues than a conventional TPM (transcript per million)-based thresholding approach (Figure S1E) and produced a set of 316 tissue-specific lncRNA genes that were detected in only one broad tissue category (Figure 1A; Table S2; STAR Methods). Tissue-specific lncRNA genes were most frequently expressed in testis, brain, blood, and skin tissues. The especially high numbers of genes preferentially expressed in the testis tissue may reflect "transcriptional scanning" during spermatogenesis (Xia et al., 2020).

Most lncRNA gene expression is influenced by genetic variation

eQTL analysis provides a systematic approach to assess the regulatory impacts of genetic variants across the transcriptome. We found that 67.3% of all 14,100 annotated lncRNA genes were eGenes, meaning that they had at least one variant significantly associated with their gene expression in at least one tissue (false discovery rate [FDR] < 0.05) (GTEx Consortium, 2020). Within each tissue, ~50% of expressed lncRNA genes were detected as eGenes, compared to ~80% of expressed protein-coding genes (Figure 1B). We observed a higher proportion of eGenes for the set of lncRNA genes with curated functions and, overall, comparable proportions across lncRNA types (Figure S1F). To assess whether lncRNA eGene discovery was limited by expression levels, we created an expression-matched protein-coding gene set within each tissue (STAR Methods) and observed that a greater percentage (~67%) of these expression-matched protein-coding genes were eGenes (Figure 1B).

Figure 1. Specificity of gene expression and presence of eQTLs across GTEx tissues

(A) The numbers of lncRNA genes with tissue-specific expression across the broad tissue categories of GTEx.

(B) Proportion of expressed genes that were eGenes (MashR LFSR < 0.05). Boxplots reflect the range of proportions across the 49 GTEx tissues.

(C) Distribution of distance between the eVariant and the gene's transcription start site for the top eQTL for each gene in each tissue. The plot is truncated at 200 kb for visibility, but the maximum outlier value was 1 Mb. Gene group differences were significant ($p < 0.05/15$, Wilcoxon test) between each lncRNA group and the protein-coding genes and the expression-matched coding genes, but not between lncRNA gene groups.

(D) Absolute effect size of the top eQTL for each gene in each tissue. Effect size was measured as $\log_2$ (allelic fold change). The dashed line separates the main comparison gene groups from the lncRNA gene types. Gene group differences were significant ($p < 0.05/23$, Wilcoxon test) between all main gene groups (left of dashed line) except for expression-matched protein-coding genes versus total lncRNA genes. Between lncRNA gene types, all differences were significant except for antisense versus sense intronic and other lncRNAs, sense intronic versus other lncRNAs, and processed transcript versus sense overlapping and other lncRNAs.

(E) Summary of the π_1 replication values between GTEx lncRNA gene eQTLs and other QTL studies.

(F) Proportion of each gene group that was an eGene in a certain number of tissues. Bar labels indicate the number of genes.

(G) The number of tissues expressing protein-coding genes (left) and lncRNA genes (right) at a threshold of $\geq$0.1 TPM in >20% of samples, compared to the subset of tissue-specific eGenes. Note that the y axis is on log scale.

For all boxplots, data represented are medians with first and third quartiles as boxes, and whiskers extending to 1.5 times the interquartile range.

See also Figure S1 and Tables S1 and S2.

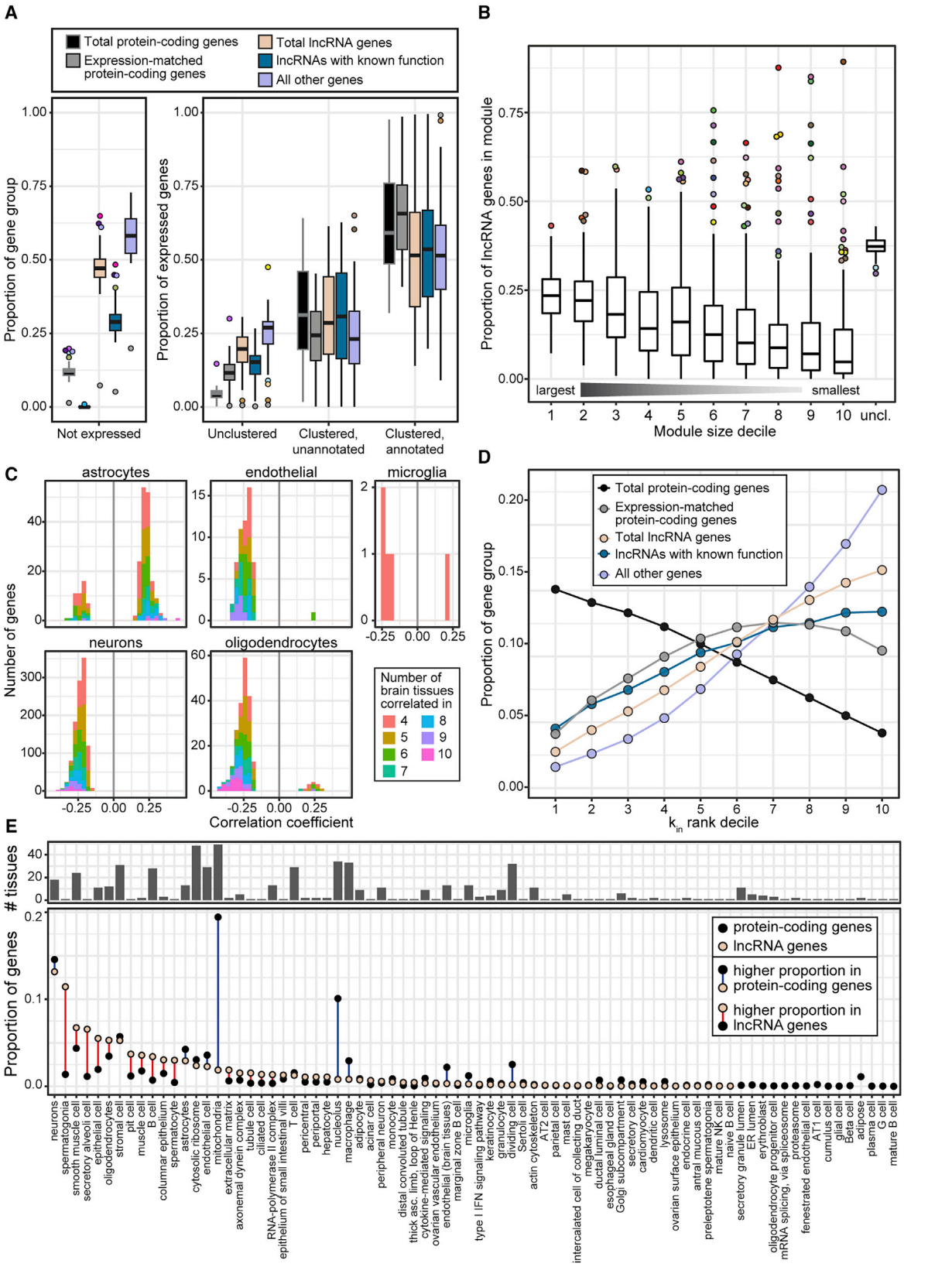

(legend on next page)

Alongside the lower abundance of lncRNA genes with eQTLs, we observed additional evidence that lncRNA genes have simpler regulatory mechanisms than protein-coding genes. First, the distance between the lead eQTL's associated variant (eVariant) and its associated gene's transcription start site (TSS) was shorter (median lncRNA eVariant-TSS distance = 21 kb versus median protein-coding eVariant-TSS distance = 32 kb; $p < 10^{-16}$, Wilcoxon test) (Figure 1C), suggesting that its regulatory mechanisms operated closer to the gene. Second, lncRNA eQTLs had higher effect sizes than protein-coding eQTLs (Figure 1D), suggesting fewer regulatory targets. This difference was partly explained by expression level, as we observed similarly high effect sizes for the expression-matched, protein-coding gene eQTLs. However, among lncRNA types, intergenic lncRNA genes had the highest eQTL effect sizes, despite having similar median expression across all tissues (median intergenic lncRNA TPM = 0.28, median lncRNA TPM = 0.34). Combined, these observations indicate that intergenic lncRNA genes have less complex regulation, supporting previous observations using massively parallel reporter assays (Mattioli et al., 2019).

We assessed replication of GTEx lncRNA eQTLs against other QTL resources using the π_1 value, an estimate of the proportion of true-positive p values. Replication of GTEx lncRNA eQTLs in other eQTL datasets for blood; EBV (Epstein-Barr virus)-transformed lymphoblastoid cell lines (LCLs); and brain, adipose, and skin tissues had a median π_1 of 0.75 (range = 0.32–0.89; Figure 1E; STAR Methods) (Buil et al., 2015; Gutierrez-Arcelus et al., 2013; Lepik et al., 2017; Ng et al., 2017; Võsa et al., 2018). To assess the replication of lncRNA eQTLs for other molecular phenotypes, we overlapped GTEx eQTLs with QTLs for epigenetic marks from both brain (frontal cortex) (Ng et al., 2017) and LCLs (Grubert et al., 2015). In the frontal cortex, where there were 1,612 lncRNA eGenes, there was a moderate overlap with QTLs for DNA methylation and H3K9 methylation (Figure 1E), illustrating the common coordination of non-coding RNA and epigenetic marks. In LCLs, where there were 932 lncRNA eGenes, overlaps with QTLs for DNase I-hypersensitivity sites, H3K27 acetylation, H3K4 monomethylation, and H3K4 trimethylation were lower (Figure 1E), which was predominantly related to differences in power and methods used for each study. Combined, these epigenetic QTL overlaps highlight many candidate regulatory connections influencing lncRNA expression.

Of the discovered lncRNA eGenes, we observed that 2,783 had evidence of tissue specificity (STAR Methods). This was more than was seen in protein-coding genes (Figure 1F), with testis, skin, blood, thyroid, and brain having the highest numbers (Table S2). Furthermore, we observed that this tissue specificity was not solely driven by tissue-specific expression levels, as 15% of tissue-specific eGenes were expressed in all tissue categories (Figures 1G and S1G). Across the tissues, this ranged from 6% (testis) to 100% (uterus) of their tissue-specific eGenes being expressed in in all tissue categories (median = 24%), demonstrating tissue specificity of lncRNA genetic regulatory effects.

Co-expression networks annotate cellular contexts of lncRNA genes

To improve our understanding of the cellular contexts of lncRNA genes, we performed weighted gene co-expression network analysis (WGCNA) (Langfelder and Horvath, 2008) within each GTEx tissue and annotated these co-expression modules to specific cell types or compartments using existing single-cell datasets (Figures S2A and S2B; Data S1; STAR Methods). On average, 80% of sufficiently expressed lncRNA genes were assigned to a module (Figure 2A; STAR Methods). We noted that larger modules included higher proportions of lncRNA genes (Figure 2B); however, there were also some smaller modules mostly made up of lncRNA genes, which may represent hubs of lncRNA regulatory activity. For example, the adrenal gland, tibial artery, minor salivary gland, pancreas, and uterus tissues each had a small, unannotated co-expression module that was 75%–89% lncRNA genes. There were 23 genes shared across the modules of these five tissues, 21 of which were lncRNA genes; these genes were widely spread across chromosomes, suggesting that this lncRNA-dominated group of co-expressed genes is not simply mediated by proximity and might be performing a similar role within each of these tissues.

We used these co-expression networks to refine the cellular contexts of tissue-shared and -specific lncRNA eGenes. We observed that, relative to all lncRNA genes, tissue-shared eGenes were enriched for the cell-compartment annotations of mitochondria and cytosolic ribosomes, for the pathway annotation of type I interferon signaling pathway, and for the stomach cell-type annotations of parietal cell and antral mucus cell (all odds ratios [ORs] > 1.5 and ps < 0.05, Fisher's test). In contrast,

Figure 2. Co-expression networks annotate cellular contexts of lncRNA genes

(A) Summary of gene assignment to modules by gene group. The underlying boxplot indicates the proportion of a gene group falling into that module status across tissues. Outlier point color indicates the tissue.

(B) Proportion of lncRNA genes in modules across all tissues, binned by module size. uncl., unclustered genes.

(C) lncRNA genes with high confidence annotations in brain tissues, based on agreement of WGCNA annotations and correlation with CIBERSORTx estimated cell-type proportions. The correlation coefficient is the median correlation across all relevant brain tissues between the estimated proportion of that cell type and the lncRNA gene's expression. The bar fill indicates the number of brain tissues in which the lncRNA gene's expression level was significantly correlated with the estimated cell-type proportion.

(D) Proportion of gene groups binned by intra-modular connectivity (k_{in}) ranking. The most highly connected genes within their module are in the first k_{in} rank decile, and the least connected genes within their module are in the 10th k_{in} rank decile.

(E) Module annotations of genes in the top k_{in} rank decile of their modules. The bottom panel indicates the proportion of these highly connected genes in each annotation group. The top panel indicates the number of tissues in which a module is assigned that annotation term. In some cases, the association of many highly connected genes with a certain annotation term may reflect how common that module is across tissues: for example, there is at least one "mitochondria" module in all 49 tissues, which may result in the same hub genes for mitochondria being counted multiple times.

For all boxplots, data represented are medians with first and third quartiles as boxes and whiskers extending to 1.5 times the interquartile range.

See also Figures S2 and S3, Data S1, and Table S3.

enriched module annotations for tissue-specific eGenes were dominated by sperm cell terms, which was consistent with many of these eGenes being specific for the testis tissue. Other enriched annotations in the tissue-specific eGenes included monocytes and megakaryocytes, keratinocytes, hepatocytes, and cardiomyocytes (OR > 1.5 and $p < 0.05$, Fisher's test).

Since gene co-expression clustering in bulk tissues can be driven by cell composition, we further incorporated estimated cell proportions in the brain and blood tissues into co-expression analyses to identify the subset of lncRNA genes where both module and cell-type proportion annotations were concordant (STAR Methods). In the brain tissues, 1,554 lncRNA genes had matching annotation between the two methods, providing increased support for their cell-type annotation (Figure 2C; Table S3). These genes were mostly annotated to the more common cell types such as neurons (1,069), oligodendrocytes (215), astrocytes (209), and endothelial cells (56) (Figures S3A and S3B). In blood, 2,837 confident lncRNA blood cell-type annotations were identified (Figures S3C and S3D; Table S3), most of which were annotated to monocytes (1,567) or T cells (1,193).

To identify additional cell-type-relevant lncRNA genes, particularly in those tissues where single-cell data were not available, we used the WGCNA metric for within-module connectivity (k_{in}) to identify lncRNA genes that were highly connected within specific annotated modules (STAR Methods). We first observed that lncRNA genes were not as often highly connected compared to protein-coding genes, especially in larger co-expression modules (Figures 2D and S2C); part of this was due to a relationship between connectivity and expression level (Figure S2D). Relative to the total group of lncRNA genes, antisense lncRNA genes were enriched for being highly connected, while intergenic lncRNA genes were depleted (antisense OR = 2.10, $p < 10^{-16}$; intergenic OR = 0.88, $p = 2.3 \times 10^{-3}$; Fisher's test). Focusing on the most highly connected lncRNA and protein-coding genes (genes in the top k_{in} decile in their assigned module), we identified the neuron module as a common annotation for both gene groups, and highly connected lncRNA genes were additionally frequently assigned to early sperm cells, muscle cells, epithelium, and tissue-resident B cells (Figures 2E and S2E).

Intergenic lncRNA genes are enriched for having high allele-specific expression (ASE) that is shared with their neighboring genes

ASE, as measured by the imbalance of expressed alleles in RNA-sequencing data, can provide an additional means to detect *cis*-acting regulatory variation. We observed 3,871 protein-coding, 1,138 intergenic lncRNA, and 863 antisense lncRNA genes with high ASE (mean gene *Z* score > 3) (Table S4). Compared to protein-coding genes, both lncRNA gene groups were enriched for high ASE (intergenic OR = 1.67, $p < 10^{-16}$; antisense OR = 1.34, $p = 3.8 \times 10^{-11}$; Fisher's test).

As some lncRNAs can operate on large genomic intervals that are detectable through ASE patterns—e.g., *XIST* (Brown et al., 1991; Engreitz et al., 2013)—we sought to test local patterns of ASE for lncRNA genes. To assess this, we defined local sharing events, where ASE was present for both the lncRNA gene and adjacent genes within a 500-kb neighboring window (mean gene *Z* score > 3, and mean neighbor *Z* score > 3) (Figure 3A; STAR Methods). In total, we identified 137 genes with high ASE sharing that was consistent across tissues. Among these genes, there was an enrichment in intergenic lncRNA genes relative to protein-coding genes, while antisense lncRNA genes were slightly depleted for high ASE-sharing events (Figure 3B). We further identified 16 lncRNA genes (15 intergenic, 1 antisense) that were the only genes in their neighborhood to have a mean neighbor *Z* score (>3). Although some of the genes around these lncRNAs showed ASE, they did not have high neighbor *Z* scores, indicating the potential for these lncRNAs to have *cis*-acting impacts on their local regulatory regions (Figure 3C).

Rare variation impacts intergenic lncRNA gene expression and complex traits

Rare genetic variation influences risk for both rare and common diseases (Keinan and Clark, 2012), and thousands of rare variants are present in each human genome (Auton et al., 2015; Bomba et al., 2017; Wright et al., 2018). We sought to define the properties of rarer genetic variants influencing lncRNA gene expression by applying an outlier enrichment approach (Ferraro et al., 2020). We first identified 1,563 intergenic lncRNA multi-tissue outlier events, with an outlier event being an individual-gene combination that was an outlier for the majority of that individual's sampled tissues (|median *Z* score| > 2) (Table S5; STAR Methods). We then focused on the 1,119 outliers involving intergenic lncRNA genes with detectable expression in all tissues; for these widely expressed genes, a multi-tissue outlier individual is more likely a reflection of consistent transcriptional differences rather than spurious detection in a few tissues. These outlier events involved 497 unique intergenic lncRNA genes and 545 unique individuals. There were 23 instances of shared multi-tissue outlier events between an intergenic lncRNA gene and a protein-coding gene within 10 kb of each other; 14 of these outlier events involved a nearby rare variant, and three of these lncRNA/protein-coding gene outlier pairs occurred in more than one individual (Figures S4A and S4B). Relative to all tested genes, intergenic lncRNA genes were less likely to have any outlier individuals (Figure S4C). The majority of intergenic lncRNA outliers were overexpression outliers (Figure 4A). This may be partially due to lncRNA genes' generally lower expression, since lowly expressed genes are more likely to fluctuate upward, and their under-expression is difficult to detect.

Intergenic lncRNA gene outlier events were enriched for the presence of nearby genetic variants, particularly for rare variants (minor allele frequency < 1% in GTEx and gnomAD non-Finnish Europeans) (Karczewski et al., 2020) and especially for rare structural variants (SVs). This was assessed by relative risk (RR; the proportion of outlier individuals with variant/proportion of non-outlier individuals with variant); RRs were 1.14 for SNVs, 1.31 for small insertions or deletions (indels), and 16.52 for structural variants, with increasing enrichments at higher *Z* score thresholds (Figure 4B). In contrast to protein-coding genes, we observed that most of the enrichment was driven by the overexpression outliers (Figure S4D). Overall, 55% of the intergenic lncRNA outlier events in tested individuals were associated with a nearby rare variant.

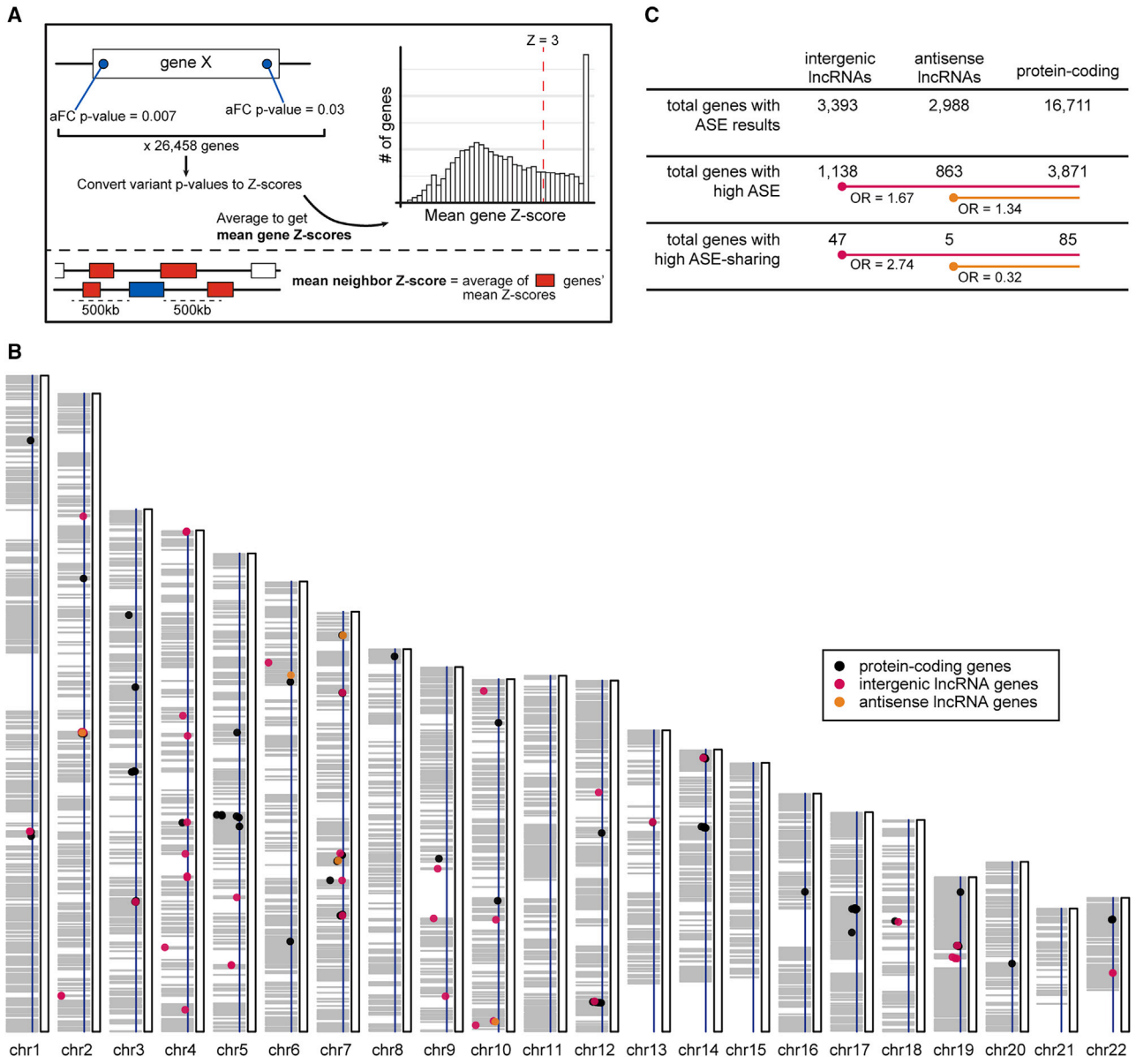

Figure 3. Patterns in allele-specific expression (ASE) associated with lncRNA gene eQTLs

(A) Scheme for calculating gene-level and neighbor gene-level ASE scores. aFC, allelic fold change.

(B) ASE-sharing results for genes, grouped by gene type. Odds ratios (ORs) were calculated for the lncRNA gene types relative to the protein-coding genes, with the background being total genes with ASE results; all were significant at $p < 0.05$, Fisher's test. High ASE, mean gene Z score > 3; High ASE-sharing, mean gene Z score > 3 and mean neighbor Z score > 3.

(C) Genome-wide distribution of high ASE-sharing genes. A dot's horizontal position indicates its mean neighbor Z score, with a further left dot having a higher Z score and the blue horizontal line marking the $Z = 3$ threshold. The gray shading illustrates stretches of the genome where, starting from a given gene with high ASE, at least one other gene within 500 kb also has high ASE.

See also Table S4.

We further stratified rare variant enrichments across different variant subclasses to refine identification of variant properties driving lncRNA outliers. Deletions, copy number variations (CNVs), and duplications were all specifically enriched in outlier individuals near their outlier genes (Figure 4C). Notably, splice variants were also strongly enriched near outlier genes (RR = 68.3, $p < 10^{-16}$)—even more so than rare TSS variants (RR = 15.1, $p < 10^{-16}$). This is consistent with a similarly strong enrichment for rare splice variants observed near protein-coding gene outliers (Ferraro et al., 2020), as well as the strong enrichment of splice-related annotations for *cis*-eQTLs, including those that were distinct from splicing quantitative trait loci (sQTLs) (GTEx Consortium, 2020). Although several different rare variant classes had strong enrichment near intergenic lncRNA outliers, these

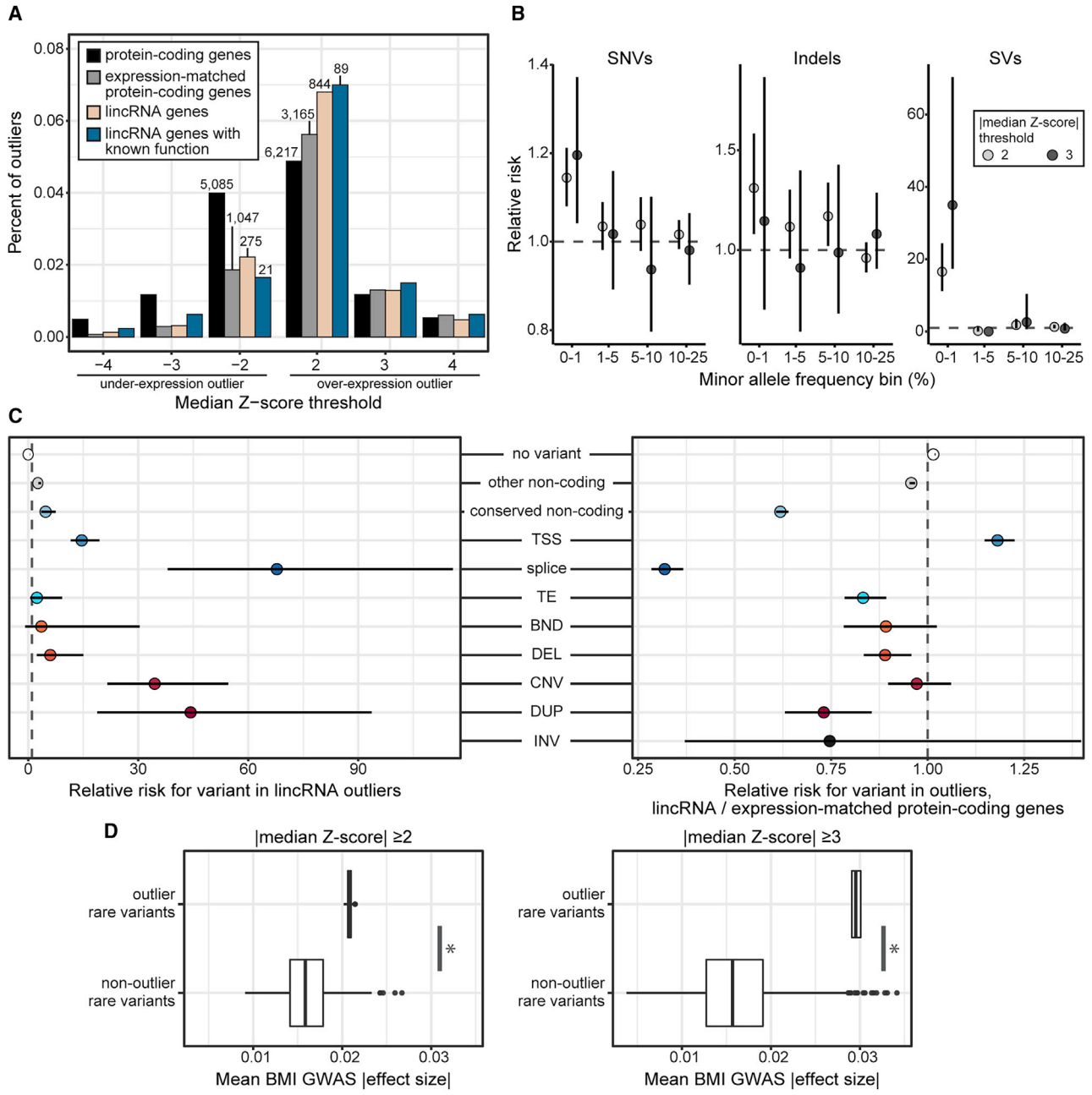

Figure 4. Rare variation impacts intergenic lncRNA gene expression and complex traits

(A) Percentage of multi-tissue intergenic lncRNA gene outliers out of all gene-individual combinations tested. Labels indicate the number of outliers.

(B) Enrichment of variants within 10 kb of the outlier gene in outlier individuals. Dots represent relative risk point estimate, with bars indicating the 95% confidence intervals.

(C) Enrichment of rare variants (minor allele frequency < 1%) within 10 kb of the outlier gene in outlier individuals. Left panel: the enrichment of rare variants in intergenic lncRNA outliers relative to non-outliers. Right panel: the enrichment values from the left relative to those same enrichment values for expression-matched protein-coding genes. Data are represented as in (B).

(D) The mean effect size in the UK Biobank GWAS for body mass index of rare variants associated with intergenic lncRNA gene expression outlier events, compared to matched rare variants associated with non-outlier events. The heightened GWAS effect size of outlier-associated variants increases with gene expression outlier *Z* score (left and right panels). * $p < 0.05$, Wilcoxon test. The boxplot represents medians with first and third quartiles as boxes and whiskers extending to 1.5 times the interquartile range.

lincRNA, intergenic lncRNA; TSS, transcription start site; TE, transposable element insertion; BND, breakend; DEL, deletion; CNV, copy number variation; DUP, duplication; INV, inversion.

See also Figure S4 and Table S5.

enrichments were not as strong as those for nearby expression-matched protein-coding gene outliers (Figure 4C). The exception was TSS variants, which had significantly stronger enrichment in lncRNA gene outliers (RR = 1.19, $p < 10^{-16}$); this is consistent with our findings from the eQTL analysis that lncRNA gene expression is regulated by simpler mechanisms than protein-coding genes.

Using the pool of rare variants identified from lncRNA outliers, we sought to test whether these variants were enriched for subsequent impacts on complex traits. We identified 44 rare variants that were near lncRNA gene outliers, not near protein-coding gene outliers, and present in the UK Biobank. For comparison, we made a control, non-outlier pool of 3,173 rare variants that were near the same lncRNA genes but only present in individuals who were not outliers for those genes (|median Z score| < 1). We observed that outlier-associated rare variants had higher effect sizes in the UK Biobank GWAS for body mass index compared to non-outlier rare variants ($p < 0.05$, Wilcoxon test) (Figure 4D). Although it may be expected that rare variants can have major impacts on a single gene's expression, these analyses provide evidence that the rare variants associated with intergenic lncRNA gene expression influence common complex traits.

Colocalization of QTL and GWAS signals creates a catalog of trait-associated lncRNA genes

Discovering the trait and disease relevance of lncRNA genes has been a major challenge, with only a few examples robustly connected to phenotypic consequences (Wapinski and Chang, 2011). To address this challenge, we systematically assessed the roles of all lncRNA genes across a diverse set of traits through colocalization analyses. Following the standards of the recent GTEx GWAS analysis (Barbeira et al., 2021; GTEx Consortium, 2020), we combined multiple colocalization approaches to improve performance: SMR+HEIDI (Zhu et al., 2016), FINEMAP+eCAVIAR (Benner et al., 2016; Hormozdiari et al., 2016), and *coloc* (Giambartolomei et al., 2014). By assessing 101 traits from 176 GWASs (Figure S5A; Table S6) for both expression and splicing QTLs, we provide a comprehensive evaluation of the roles of lncRNA genes in complex traits and disease.

We identified 1,432 significant lncRNA colocalization events, significantly expanding the lexicon of trait-associated lncRNA genes (Table S6). We defined a "colocalization event" as a robust relationship between a feature (such as a gene for eQTLs or a splice cluster for sQTLs) and a GWAS locus in a certain tissue. Together, these colocalization events encompassed 69 traits and 166 lncRNA features (119 genes, 47 splice clusters). As a point of reference, there were 9,167 significant protein-coding gene colocalization events, involving 82 traits and 1,096 unique features (416 genes, 680 splice clusters). Some trait categories had high proportions of lncRNA eQTL colocalization events, including lupus, multiple sclerosis, and blood cell counts (Figures 5A and S5B). For other traits, such as amyotrophic lateral sclerosis, Parkinson's disease, and substance use, no lncRNA colocalization events were observed for either QTL type. In these cases, there were few colocalized QTLs for any gene type; many of the GWAS within these trait categories had low numbers of candidate variants, which limited the number of QTL-GWAS colocalizations that our analyses could detect.

For eQTL colocalization events, 19% of all unique lncRNA gene-GWAS discoveries were shared across all three colocalization approaches (Figure 5B). *coloc* yielded the highest number of eQTL colocalization discoveries (264), followed by FINEMAP+eCAVIAR (187), and SMR+HEIDI was the most conservative (75) (see STAR Methods for the thresholds of each colocalization approach). Compared to protein-coding genes, colocalizations with sQTLs for lncRNA genes were rare, due to the low abundance of lncRNA sQTLs (Figure 5B).

Working with multi-tissue QTL data provides the unique opportunity to identify lncRNA genes with the strongest evidence for colocalization compared to any nearby protein-coding genes in the same or a different tissue. We first evaluated whether the lncRNA gene's colocalization score was greater than that of any protein-coding gene in its surrounding 1-Mb range. Subsequently, we calculated a metric for how much better the lncRNA gene's colocalization score was than that of adjacent genes (Table S6; STAR Methods). We detected 574 (40%) lncRNA colocalization events (feature-GWAS-tissue combinations) that were surrounded by genes that either could not be tested for colocalization (for example, if they had no QTLs) or did not have a significant colocalization for the same GWAS in that same tissue (Figures 5C and S5C). An additional 226 (16%) events had neighboring genes with colocalizations that were significant, but with a weaker colocalization than the lncRNA gene, for a total of 800 lncRNA colocalization events with the strongest colocalization score in their 1-Mb region within a given tissue. Notably, we found that these included 120 unique lncRNA feature-GWAS combinations that met the more stringent requirement of having the strongest colocalization score in their 1-Mb region across all tissues (Table S6).

To identify putative causal variants in lncRNA gene-trait associations, we fine-mapped variants for all FINEMAP+eCAVIAR colocalization events where a lncRNA gene had the highest colocalization posterior probability (CLPP) in a 1-Mb surrounding region (Table S6; STAR Methods). We observed differences across annotation categories in these fine-mapped variants from lncRNA colocalization events relative to a background set of all GTEx variants either located in a gene or within 400 kb of any gene: regulatory regions, such as enhancers and promoters, and non-coding exons were enriched in the set of fine-mapped variants, but these variants were also depleted for splice donor and acceptor sites, intron variants, and CTCF binding sites (Figure 5D).

To demonstrate how our combined catalog of colocalization events and cell-type annotations can generate hypotheses about lncRNA-mediated trait and disease pathways, we highlighted a colocalization between the lncRNA genes *LINC01475* (ENSG00000257582) and *RP11-129J12.1* (ENSG00000228778) and ulcerative colitis. The two genes overlap on opposite strands and are just upstream of the protein-coding gene *NKX2-3* (Figure 6A). *NKX2-3* has received attention related to the significant ulcerative colitis GWAS results in this genomic region (Lu et al., 2014). However, when looking at the colocalization scores, the two lncRNA genes have significant colocalizations with all three colocalization approaches across multiple tissues, whereas *NKX2-3* only has a single significant colocalization for one method in one tissue (Figure 6B). Additionally, the tissues in

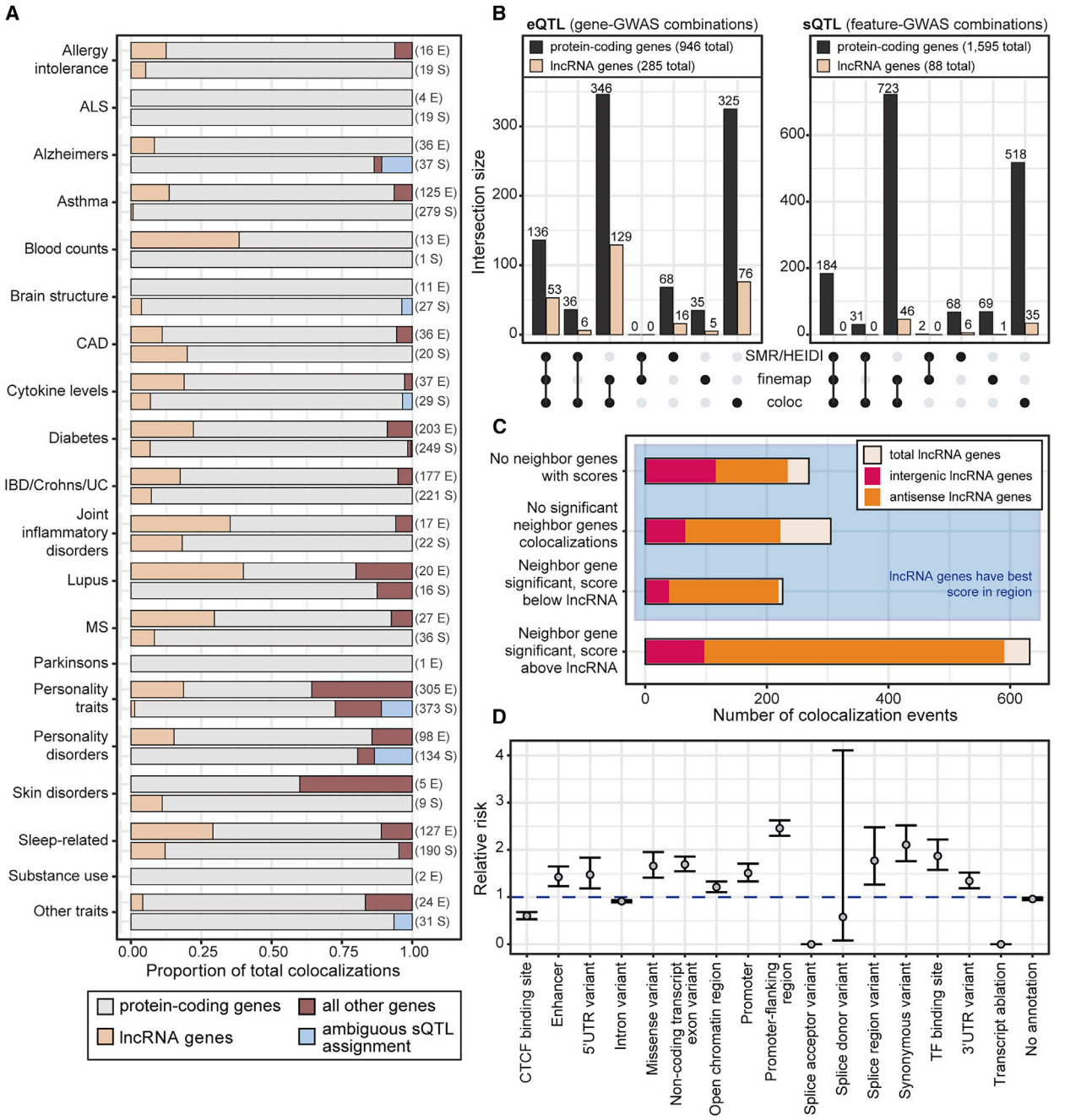

Figure 5. GWAS-QTL colocalization identifies trait-associated lncRNA genes

(A) Contribution of each gene type to significant colocalization events, collapsed across tissues (feature-GWAS combinations). GWAS were grouped on the y axis by general trait categories. For each trait category, the top bar indicates eQTL colocalizations, and the bottom bar indicates sQTL colocalizations. If a bar is missing from the plot, there were no colocalizations for that given trait category and QTL type. The numbers at the right of each bar indicate the total number of significant colocalization events (E, eQTL; S, sQTL). ALS, amyotrophic lateral sclerosis; CAD, coronary artery disease; IBD, inflammatory bowel disease; UC, ulcerative colitis; MS, multiple sclerosis.

(B) Number of significant colocalization events collapsed across tissues (feature-GWAS combinations) for each approach.

(C) Significant lncRNA colocalization events (feature-GWAS-tissue combinations) grouped by the colocalization status of protein-coding genes in the surrounding 1-Mb range.

(D) Enrichment of variant annotation categories in the 95% credible sets of all significant lncRNA colocalization events discovered by FINEMAP. Enrichment was calculated relative to all GTEx variants that were not within the credible set and were within 400 kb of an annotated gene. Dots represent relative risk point estimate, with bars representing the 95% confidence intervals.

See also Figure S5 and Table S6.

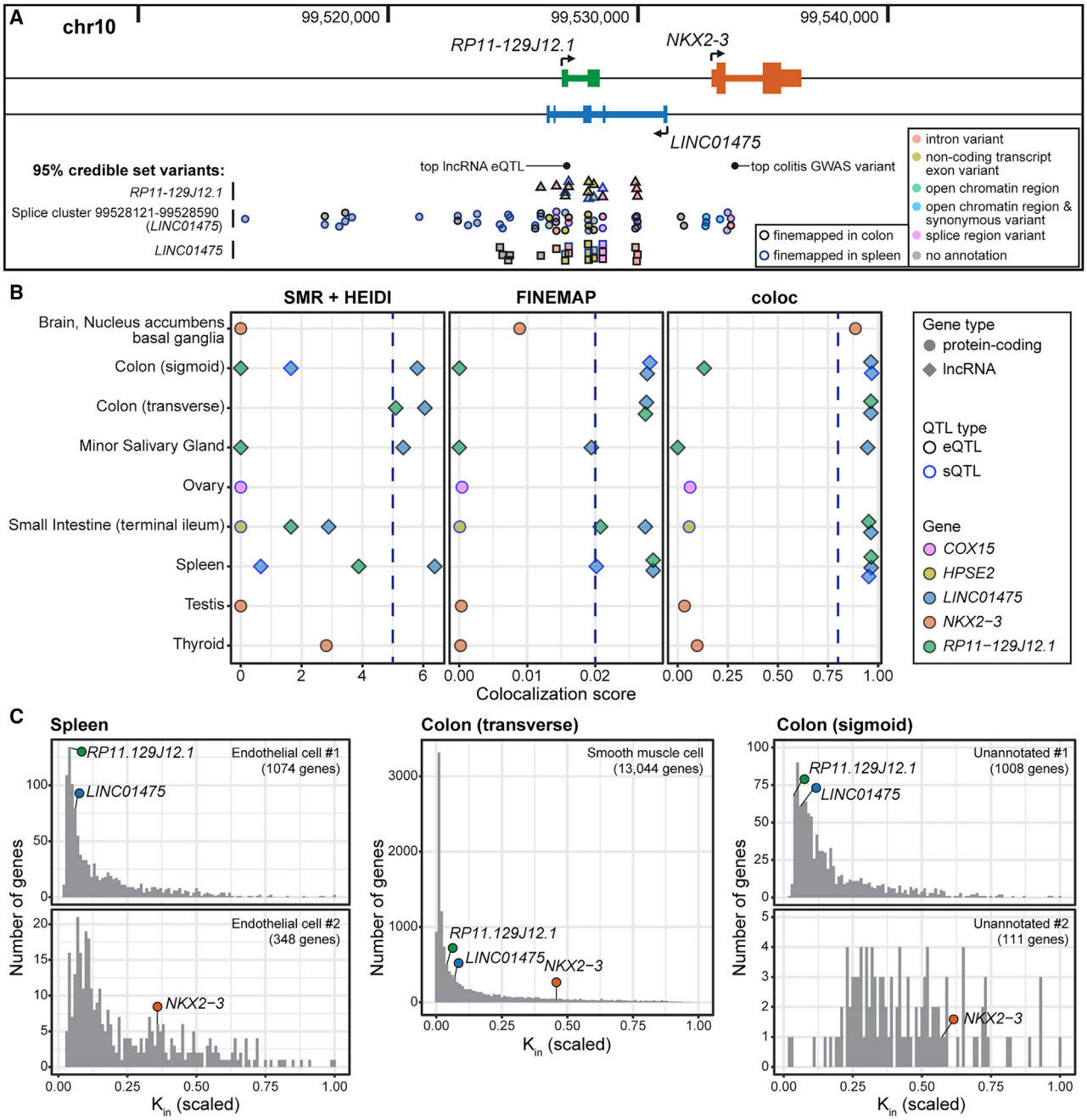

Figure 6. Exemplar significant colocalization of *LINC01475* and *RP11-129J12.1* with ulcerative colitis

(A) Location of the lncRNA genes and the nearby protein-coding gene *NKX2-3*. Relevant variants are labeled, including the most significant ulcerative colitis GWAS variant, and the top eQTL for both lncRNA genes in the transverse colon, as well as the 95% credible sets for the FINEMAP colocalizations in spleen and colon tissues involving a *RP11-129J12.1* eQTL (triangles), a *LINC01475* sQTL (circles), and a *LINC01475* eQTL (squares).

(B) Summary of colocalization scores for ulcerative colitis for the lncRNA genes and genes in the surrounding 1 Mb; 14 genes had no score in any tissue and are not indicated. The thresholds for significant colocalization are indicated by the blue dashed lines (STAR Methods).

(C) Scaled intramodular connectivity (k_{in}) of *LINC01475*, *RP11-129J12.1*, and *NKX2-3* within their assigned modules in the gene co-expression networks for spleen, transverse colon, and sigmoid colon. Module annotation and size are indicated in the top right corner of each panel.

See also Table S6.

which the lncRNA genes colocalize have relevance to ulcerative colitis: intestinal tissues (sigmoid colon, transverse colon, and small intestine); the spleen, which could be connected via immune system regulation; and the minor salivary gland (Muhvić-Urek et al., 2016). In contrast, the sole colocalization for *NKX2-3* occurs in a single brain tissue (nucleus accumbens, basal ganglia). These patterns of colocalizations were also observed for GWAS from inflammatory bowel disease and Crohn's disease, indicating that the regulatory pathway is involved in the development of both ulcerative colitis and Crohn's disease.

Within the cell-type annotations, all three genes were assigned to the same "smooth muscle cell" module in the transverse colon co-expression network, while in the spleen co-expression network, *NKX2-3* was assigned to one "endothelial cell" module, and the two lncRNA genes were assigned to a different "endothelial cell" module (Figure 6C). *NKX2-3* is a homeobox gene that is key for the development of the spleen and the visceral mesoderm, which develops several essential cell types of the gastrointestinal tract, including endothelial cells, immune cells, and—notably—smooth muscle cells. Knockout mouse studies have shown that loss of this gene affects spleen architecture, as well as lymphocyte maturation and homing (Pabst et al., 1999, 2000; Robles et al., 2016; Tarlinton et al., 2003; Vojkovics et al., 2018). When combined with the colocalization data, this suggests that the functions of these two lncRNAs, through regulation of *NKX2-3*, in both the colon and spleen influence ulcerative colitis susceptibility.

DISCUSSION

Genetic studies of gene expression have significantly contributed to the identification of the molecular basis of diverse complex traits (Albert and Kruglyak, 2015). To date, the majority of this effort has focused on regulatory effects of non-coding sequences on protein-coding genes, instead of on non-coding genes such as lncRNA genes. Recent advances in population-scale transcriptomics across human tissues from GTEx (GTEx Consortium, 2020) combined with growing resources from GWAS (Buniello et al., 2019) and population biobanks (Bycroft et al., 2018), now provide the means to systematically incorporate lncRNA genes into these endeavors. To this end, we have assessed the regulatory patterns of lncRNA genes and significantly expanded annotation of their potential roles in specific cellular contexts and across diverse complex traits and diseases. The multi-tissue aspect of the GTEx data allowed us to address a major challenge of identifying trait and disease associations that were specific to lncRNA genes and not, instead, driven by protein-coding genes in other tissue contexts.

The GTEx v8 data provide extensive annotation of genetic effects impacting lncRNA genes, identifying eQTLs for 67.3% of all 14,100 annotated lncRNA genes (GTEx Consortium, 2020). However, a major challenge with multi-tissue eQTL data has been assessing the degree of tissue specificity of genetic effects (Urbut et al., 2019). Our work demonstrated that tissue specificity of lncRNA gene expression can be influenced by how specificity is defined, and we add to evidence of more widespread lncRNA gene expression. In addition, we observed that lncRNA eQTLs can be tissue specific, even when the genes are expressed across all tissue types, with 8.8% of lncRNA tissue-specific eGenes expressed in all broad tissue categories. Combined, the GTEx catalog of lncRNA eQTLs greatly expands the annotation of genetic variants influencing lncRNA gene expression and highlights the role of genetic variation in contributing to tissue specificity.

A complement to multi-tissue transcriptome data has been ongoing efforts to map cellular identities using single-cell-sequencing techniques (Darmanis et al., 2015; Han et al., 2018; Regev et al., 2017). Combining these data now provides an opportunity to refine cell-type annotations of lncRNA genes. We integrated co-expression analysis with single-cell gene expression reference maps and provide cell type and compartment annotations for 94.4% of lncRNA genes in at least one tissue. These data provide a resource for understanding the cellular contexts of lncRNA genetic effects and subsequently identifying their pathological cellular contexts in diverse diseases.

Both rare and common variants have the potential to impact complex traits and diseases. However, the involvement of genetic variants impacting lncRNA genes and contributing to complex disease remains difficult to ascertain. Examples of prominent rare variants impacting lncRNA genes in disease have included prostate cancer (Walavalkar et al., 2020), HELLP syndrome (van Dijk et al., 2015), and limb malformation (Allou et al., 2021). By applying gene expression outlier analysis, we were able to identify rare variants that impact lncRNA genes and connect those effects to body mass index, a highly polygenic trait. To systematically map lncRNA genes to complex traits and diseases, we applied colocalization analysis combining common GWAS, eQTL, and sQTL genetic variants across 14,100 lncRNA genes, 101 traits, and 49 tissues using three approaches. We identified 800 lncRNA colocalization events in which there was no stronger protein-coding colocalization within 1 Mb; notably, this included 120 unique lncRNA-GWAS combinations in which no nearby protein-coding genes had a greater colocalization score in any tissue. These colocalization events represent robust connections between genetic variation, lncRNA gene expression, and complex traits. While dissecting the functional impacts of even a single lncRNA gene has been a major challenge, by combining these analyses with enhanced cell-type classifications, we have generated a comprehensive catalog of trait-associated lncRNA genes and their cellular contexts.

Limitations of study

Although this multi-tissue dataset allowed us to identify lncRNA genes with robust connection to cell types and complex diseases, targeted assessment of the cellular and organismal impacts of disease-associated lncRNAs in model systems would further confirm our findings. Additionally, developmental and environmental influences such as immune responsivity, behavior, and medication can impact gene expression and may have different regulatory genetic effects that were not well captured in the GTEx cohort, limiting our ability to catalog the impacts of disease risk variants in all potential contexts. Despite these limitations, these findings significantly extend the

discovery of lncRNA genes with potential impacts on human traits and diseases.

STAR★METHODS

Detailed methods are provided in the online version of this paper and include the following:

- KEY RESOURCES TABLE
- RESOURCE AVAILABILITY
  - Lead contact
  - Materials availability
  - Data and code availability
- EXPERIMENTAL MODEL AND SUBJECT DETAILS
  - GTEx subjects
- METHOD DETAILS
  - Biospecimen collection
  - Molecular analyte extraction and QC
- QUANTIFICATION AND STATISTICAL ANALYSIS
  - GTEx data
  - Defining gene groups
  - Assessing tissue-specificity of gene expression
  - Identifying independent cis-eQTLs and cis-sQTLs by forward stepwise regression-backward selection
  - Identifying tissue-shared cis-eQTLs with mash
  - Assessing replication of GTEx lncRNA eQTLs
  - Assessing overlap of GTEx lncRNA eQTLs with other studies' epigenetic QTLs
  - Weighted gene correlation network analysis (WGCNA)
  - Co-expression network module annotation via gene set enrichment
  - Cell type annotation sources
  - Identifying lncRNA genes with high confidence cell type annotations in brain and blood tissues
  - Allele-specific expression (ASE)
  - Multi-tissue gene expression outlier discovery
  - GWAS sources and data preparation for colocalization analysis
  - Selecting colocalization tests
  - Colocalization approaches: SMR + HEIDI
  - Colocalization approaches: FINEMAP
  - Colocalization approaches: coloc
  - Integrating and interpreting the colocalization results

SUPPLEMENTAL INFORMATION

Supplemental information can be found online at https://doi.org/10.1016/j.cell.2021.03.050.

CONSORTIA

The members of the GTEx Consortium who are not listed in the primary author list are Shankara Anand, Stacey Gabriel, Gad A. Getz, Aaron Graubert, Kane Hadley, Robert E. Handsaker, Katherine H. Huang, Xiao Li, Daniel G. MacArthur, Samuel R. Meier, Jared L. Nedzel, Duyen T. Nguyen, Ayellet V. Segrè, Ellen Todres, Brunilda Balliu, Rodrigo Bonazzola, Andrew Brown, Donald F. Conrad, Daniel J. Cotter, Nancy Cox, Sayantan Das, Emmanouil T. Dermitzakis, Jonah Einson, Barbara E. Engelhardt, Eleazar Eskin, Elise D. Flynn, Laure Fresard, Eric R. Gamazon, Diego Garrido-Martín, Nicole R. Gay, Roderic Guigó, Andrew R. Hamel, Yuan He, Paul J. Hoffman, Farhad Hormozdiari, Lei Hou, Brian Jo, Silva Kasela, Seva Kashin, Manolis Kellis, Alan Kwong, Xin Li, Yanyu Liang, Serghei Mangul, Pejman Mohammadi, Manuel Muñoz-Aguirre, Andrew B. Nobel, Meritxell Oliva, Yongjin Park, Princy Parsana, Ferran Reverter, John M. Rouhana, Chiara Sabatti, Ashis Saha, Matthew Stephens, Barbara E. Stranger, Nicole A. Teran, Ana Viñuela, Gao Wang, Fred Wright, Valentin Wucher, Yuxin Zou, Pedro G. Ferreira, Gen Li, Marta Melé, Esti Yeger-Lotem, Debra Bradbury, Tanya Krubit, Jeffrey A. McLean, Liqun Qi, Karna Robinson, Nancy V. Roche, Anna M. Smith, David E. Tabor, Anita Undale, Jason Bridge, Lori E. Brigham, Barbara A. Foster, Bryan M. Gillard, Richard Hasz, Marcus Hunter, Christopher Johns, Mark Johnson, Ellen Karasik, Gene Kopen, William F. Leinweber, Alisa McDonald, Michael T. Moser, Kevin Myer, Kimberley D. Ramsey, Brian Roe, Saboor Shad, Jeffrey A. Thomas, Gary Walters, Michael Washington, Joseph Wheeler, Scott D. Jewell, Daniel C. Rohrer, Dana R. Valley, David A. Davis, Deborah C. Mash, Mary E. Barcus, Philip A. Branton, Leslie Sobin, Laura K. Barker, Heather M. Gardiner, Maghboeba Mosavel, Laura A. Siminoff, Paul Flicek, Maximilian Haeussler, Thomas Juettemann, W. James Kent, Christopher M. Lee, Conner C. Powell, Kate R. Rosenbloom, Magali Ruffier, Dan Sheppard, Kieron Taylor, Stephen J. Trevanion, Daniel R. Zerbino, Nathan S. Abell, Joshua Akey, Lin Chen, Kathryn Demanelis, Jennifer A. Doherty, Andrew P. Feinberg, Kasper D. Hansen, Peter F. Hickey, Farzana Jasmine, Lihua Jiang, Rajinder Kaul, Muhammad G. Kibriya, Jin Billy Li, Qin Li, Shin Lin, Sandra E. Linder, Brandon L. Pierce, Lindsay F. Rizzardi, Andrew D. Skol, Kevin S. Smith, Michael Snyder, John Stamatoyannopoulos, Hua Tang, Meng Wang, Latarsha J. Carithers, Ping Guan, Susan E. Koester, A. Roger Little, Helen M. Moore, Concepcion R. Nierras, Abhi K. Rao, Jimmie B. Vaught, and Simona Volpi.

ACKNOWLEDGMENTS

We thank the Montgomery and Kirkegaard labs for their feedback on this work. The GTEx project was supported by the Common Fund of the Office of the Director of the National Institutes of Health (NIH) and by the National Cancer Institute, the National Human Genome Research Institute (NHGRI), the National Heart, Lung, and Blood Institute (NHLBI), the National Institute on Drug Abuse (NIDA), the National Institute of Mental Health, and the National Institute of Neurological Disorders and Stroke. We are thankful for support from a Stanford graduate fellowship and Bio-X Stanford interdisciplinary graduate fellowship (to O.M.d.G.); a National Science Foundation graduate research fellowship (to N.M.F.); NHLBI grant R01HL135313-01 (to A.S.R.); National Library of Medicine (NLM) training grant 5T15LM007033-36 (to T.Y.E.); NHLBI grant HHSN268201000029C and NHGRI grant 5U41HG009494 (to F.A. and K.G.A.); NIH grants R01GM122924 (to S.E.C. and T.L.) and 1K99HG009916-01 (to S.E.C.); Marie-Skłodowska Curie fellowship H2020 grant 706636 (to S.K.-H.); NIH grant R01HG010067 (to Y.P.); a Mr. and Mrs. Spencer T. Olin fellowship for women in graduate study (to A.J.S.); NIH grant R01MH109905 (to A.B.); the Searle Scholar Program (to A.B.); NIH grant R01MH101822 (to C.D.B.); NIH grants R01MH106842, R01HL142028, UM1HG008901, and R01GM124486 (to T.L.); NIH grants R01MH107666 and P30DK020595 (H.K.I.); NIH grants R01HL109512, R01HL134817, R33HL120757, and R01HL139478 (to T.Q.); the Chan Zuckerberg Foundation-Human Cell Atlas Initiative (to T.Q.); Stanford University School of Medicine (to K.K.); and NIH grants R01MH101814 (NIH Common Fund; GTEx Program) (to A.B. and S.B.M.), R01HG008150 (NHGRI; Non-Coding Variants Program) (to A.B. and S.B.M.), and R01AG066490, R01HL142015, U01HG009431, and U01HG009080 (to S.B.M.).

AUTHOR CONTRIBUTIONS

O.M.d.G. designed the study, conducted analyses, visualized data, and co-wrote the manuscript; D.C.N. conducted co-expression and ASE analyses. N.M.F. conducted outlier analysis and contributed to writing. M.J.G. conducted colocalization analysis. A.S.R. contributed to colocalization analysis. C.S. contributed to outlier analysis. T.Y.E. contributed to ASE analysis. F.A. generated QTL and ASE data. B.N. and J.X. contributed to QTL replication analyses. A.N.B. contributed to GWAS and colocalization analysis. S.E.C. generated ASE and tissue-sharing data. S.K.-H. generated tissue sharing data. Y.P. contributed to colocalization analysis. A.J.S. generated structural variant

data. B.J.S. contributed to outlier analysis. C.D.B. and X.W. led trainees and contributed to GWAS and colocalization analysis. I.M.H. led trainees and contributed to structural variant data. A.B. contributed to outlier analysis. T.L. led trainees. H.K.I. led trainees and led the GWAS analysis team. K.G.A. generated data and provided oversight of the LDACC and pipelines. S.M. led trainees and contributed to QTL replication analyses. T.Q. and K.K. helped with data interpretation. S.B.M. designed the study, led trainees, and co-wrote the manuscript.

DECLARATION OF INTERESTS

F.A. is an inventor on a patent application related to TensorQTL; S.E.C. is a co-founder and chief technology officer at Variant Bio and owns stock in Variant Bio; T.L. is on the scientific advisory board of Variant Bio, Goldfinch Bio, and GSK and owns stock in Variant Bio; and S.B.M. is on the scientific advisory board of MyOme. All other authors report no competing interests.

Received: December 10, 2019
Revised: October 16, 2020
Accepted: March 24, 2021
Published: April 16, 2021

REFERENCES

Albert, F.W., and Kruglyak, L. (2015). The role of regulatory variation in complex traits and disease. Nat. Rev. Genet. *16*, 197–212.

Allou, L., Balzano, S., Magg, A., Quinodoz, M., Royer-Bertrand, B., Schöpflin, R., Chan, W.-L., Speck-Martins, C.E., Carvalho, D.R., Farage, L., et al. (2021). Non-coding deletions identify Maenli lncRNA as a limb-specific En1 regulator. Nature. Published online February 10, 2021. https://doi.org/10.1038/s41586-021-03208-9.

Amin, V., Harris, R.A., Onuchic, V., Jackson, A.R., Charnecki, T., Paithankar, S., Lakshmi Subramanian, S., Riehle, K., Coarfa, C., and Milosavljevic, A. (2015). Epigenomic footprints across 111 reference epigenomes reveal tissue-specific epigenetic regulation of lincRNAs. Nat. Commun. *6*, 6370.

Ashburner, M., Ball, C.A., Blake, J.A., Botstein, D., Butler, H., Cherry, J.M., Davis, A.P., Dolinski, K., Dwight, S.S., Eppig, J.T., et al.; The Gene Ontology Consortium (2000). Gene ontology: tool for the unification of biology. Nat. Genet. *25*, 25–29.

Auton, A., Brooks, L.D., Durbin, R.M., Garrison, E.P., Kang, H.M., Korbel, J.O., Marchini, J.L., McCarthy, S., McVean, G.A., and Abecasis, G.R.; 1000 Genomes Project Consortium (2015). A global reference for human genetic variation. Nature *526*, 68–74.

Barbeira, A.N., Bonazzola, R., Gamazon, E.R., Liang, Y., Park, Y., Kim-Hellmuth, S., Wang, G., Jiang, Z., Zhou, D., Hormozdiari, F., et al.; GTEx GWAS Working Group; GTEx Consortium (2021). Exploiting the GTEx resources to decipher the mechanisms at GWAS loci. Genome Biol. *22*, 49.

Benjamini, Y., and Hochberg, Y. (1995). Controlling the False Discovery Rate: A Practical and Powerful Approach to Multiple Testing. J. R. Statist. Soc. B *57*, 289–300.

Benner, C., Spencer, C.C.A., Havulinna, A.S., Salomaa, V., Ripatti, S., and Pirinen, M. (2016). FINEMAP: efficient variable selection using summary data from genome-wide association studies. Bioinformatics *32*, 1493–1501.

Bomba, L., Walter, K., and Soranzo, N. (2017). The impact of rare and low-frequency genetic variants in common disease. Genome Biol. *18*, 77.

Brown, C.J., Ballabio, A., Rupert, J.L., Lafreniere, R.G., Grompe, M., Tonlorenzi, R., and Willard, H.F. (1991). A gene from the region of the human X inactivation centre is expressed exclusively from the inactive X chromosome. Nature *349*, 38–44.

Buil, A., Brown, A.A., Lappalainen, T., Viñuela, A., Davies, M.N., Zheng, H.-F., Richards, J.B., Glass, D., Small, K.S., Durbin, R., et al. (2015). Gene-gene and gene-environment interactions detected by transcriptome sequence analysis in twins. Nat. Genet. *47*, 88–91.

Buniello, A., MacArthur, J.A.L., Cerezo, M., Harris, L.W., Hayhurst, J., Malangone, C., McMahon, A., Morales, J., Mountjoy, E., Sollis, E., et al. (2019). The NHGRI-EBI GWAS Catalog of published genome-wide association studies, targeted arrays and summary statistics 2019. Nucleic Acids Res. *47* (D1), D1005–D1012.

Bycroft, C., Freeman, C., Petkova, D., Band, G., Elliott, L.T., Sharp, K., Motyer, A., Vukcevic, D., Delaneau, O., O'Connell, J., et al. (2018). The UK Biobank resource with deep phenotyping and genomic data. Nature *562*, 203–209.

Cabili, M.N., Trapnell, C., Goff, L., Koziol, M., Tazon-Vega, B., Regev, A., and Rinn, J.L. (2011). Integrative annotation of human large intergenic noncoding RNAs reveals global properties and specific subclasses. Genes Dev. *25*, 1915–1927.

Castel, S.E., Levy-Moonshine, A., Mohammadi, P., Banks, E., and Lappalainen, T. (2015). Tools and best practices for data processing in allelic expression analysis. Genome Biol. *16*, 195.

Castel, S.E., Mohammadi, P., Chung, W.K., Shen, Y., and Lappalainen, T. (2016). Rare variant phasing and haplotypic expression from RNA sequencing with phASER. Nat. Commun. *7*, 12817.

Castel, S.E., Aguet, F., Mohammadi, P., Ardlie, K.G., and Lappalainen, T.; GTEx Consortium (2020). A vast resource of allelic expression data spanning human tissues. Genome Biol. *21*, 234.

Chen, E.Y., Tan, C.M., Kou, Y., Duan, Q., Wang, Z., Meirelles, G.V., Clark, N.R., and Ma'ayan, A. (2013). Enrichr: interactive and collaborative HTML5 gene list enrichment analysis tool. BMC Bioinformatics *14*, 128.

Chen, H.-I.H., Liu, Y., Zou, Y., Lai, Z., Sarkar, D., Huang, Y., and Chen, Y. (2015). Differential expression analysis of RNA sequencing data by incorporating non-exonic mapped reads. BMC Genomics *16* (*Suppl 7*), S14.

Chiang, C., Scott, A.J., Davis, J.R., Tsang, E.K., Li, X., Kim, Y., Hadzic, T., Damani, F.N., Ganel, L., Montgomery, S.B., et al.; GTEx Consortium (2017). The impact of structural variation on human gene expression. Nat. Genet. *49*, 692–699.

Darmanis, S., Sloan, S.A., Zhang, Y., Enge, M., Caneda, C., Shuer, L.M., Hayden Gephart, M.G., Barres, B.A., and Quake, S.R. (2015). A survey of human brain transcriptome diversity at the single cell level. Proc. Natl. Acad. Sci. USA *112*, 7285–7290.

DeLuca, D.S., Levin, J.Z., Sivachenko, A., Fennell, T., Nazaire, M.-D., Williams, C., Reich, M., Winckler, W., and Getz, G. (2012). RNA-SeQC: RNA-seq metrics for quality control and process optimization. Bioinformatics *28*, 1530–1532.

Djebali, S., Davis, C.A., Merkel, A., Dobin, A., Lassmann, T., Mortazavi, A., Tanzer, A., Lagarde, J., Lin, W., Schlesinger, F., et al. (2012). Landscape of transcription in human cells. Nature *489*, 101–108.

Dobin, A., Davis, C.A., Schlesinger, F., Drenkow, J., Zaleski, C., Jha, S., Batut, P., Chaisson, M., and Gingeras, T.R. (2013). STAR: ultrafast universal RNA-seq aligner. Bioinformatics *29*, 15–21.

Dougherty, J.D., Schmidt, E.F., Nakajima, M., and Heintz, N. (2010). Analytical approaches to RNA profiling data for the identification of genes enriched in specific cells. Nucleic Acids Res. *38*, 4218–4230.

Engreitz, J.M., Pandya-Jones, A., McDonel, P., Shishkin, A., Sirokman, K., Surka, C., Kadri, S., Xing, J., Goren, A., Lander, E.S., et al. (2013). The Xist lncRNA exploits three-dimensional genome architecture to spread across the X chromosome. Science *341*, 1237973.

Faghihi, M.A., Modarresi, F., Khalil, A.M., Wood, D.E., Sahagan, B.G., Morgan, T.E., Finch, C.E., St Laurent, G., 3rd, Kenny, P.J., and Wahlestedt, C. (2008). Expression of a noncoding RNA is elevated in Alzheimer's disease and drives rapid feed-forward regulation of β-secretase. Nat. Med. *14*, 723–730.

Ferraro, N.M., Strober, B.J., Einson, J., Abell, N.S., Aguet, F., Barbeira, A.N., Brandt, M., Bucan, M., Castel, S.E., Davis, J.R., et al.; TOPMed Lipids Working Group; GTEx Consortium (2020). Transcriptomic signatures across human tissues identify functional rare genetic variation. Science *369*, eaaz5900.

Gardner, E.J., Lam, V.K., Harris, D.N., Chuang, N.T., Scott, E.C., Pittard, W.S., Mills, R.E., and Devine, S.E.; 1000 Genomes Project Consortium (2017). The Mobile Element Locator Tool (MELT): population-scale mobile element discovery and biology. Genome Res. *27*, 1916–1929.

Gautier, L., Cope, L., Bolstad, B.M., and Irizarry, R.A. (2004). affy–analysis of Affymetrix GeneChip data at the probe level. Bioinformatics *20*, 307–315.

Giambartolomei, C., Vukcevic, D., Schadt, E.E., Franke, L., Hingorani, A.D., Wallace, C., and Plagnol, V. (2014). Bayesian test for colocalisation between pairs of genetic association studies using summary statistics. PLoS Genet. *10*, e1004383.

Grubert, F., Zaugg, J.B., Kasowski, M., Ursu, O., Spacek, D.V., Martin, A.R., Greenside, P., Srivas, R., Phanstiel, D.H., Pekowska, A., et al. (2015). Genetic Control of Chromatin States in Humans Involves Local and Distal Chromosomal Interactions. Cell *162*, 1051–1065.

GTEx Consortium (2020). The GTEx Consortium atlas of genetic regulatory effects across human tissues. Science *369*, 1318–1330.

Gupta, R.A., Shah, N., Wang, K.C., Kim, J., Horlings, H.M., Wong, D.J., Tsai, M.-C., Hung, T., Argani, P., Rinn, J.L., et al. (2010). Long non-coding RNA HOTAIR reprograms chromatin state to promote cancer metastasis. Nature *464*, 1071–1076.

Gutierrez-Arcelus, M., Lappalainen, T., Montgomery, S.B., Buil, A., Ongen, H., Yurovsky, A., Bryois, J., Giger, T., Romano, L., Planchon, A., et al. (2013). Passive and active DNA methylation and the interplay with genetic variation in gene regulation. eLife *2*, e00523.

Han, X., Wang, R., Zhou, Y., Fei, L., Sun, H., Lai, S., Saadatpour, A., Zhou, Z., Chen, H., Ye, F., et al. (2018). Mapping the Mouse Cell Atlas by Microwell-Seq. Cell *173*, 1307.

Handsaker, R.E., Van Doren, V., Berman, J.R., Genovese, G., Kashin, S., Boettger, L.M., and McCarroll, S.A. (2015). Large multiallelic copy number variations in humans. Nat. Genet. *47*, 296–303.

Hansen, B.B., and Klopfer, S.O. (2006). Optimal Full Matching and Related Designs via Network Flows. J. Comput. Graph. Stat. *15*, 609–627.

Heward, J.A., and Lindsay, M.A. (2014). Long non-coding RNAs in the regulation of the immune response. Trends Immunol. *35*, 408–419.

Hon, C.-C., Ramilowski, J.A., Harshbarger, J., Bertin, N., Rackham, O.J.L., Gough, J., Denisenko, E., Schmeier, S., Poulsen, T.M., Severin, J., et al. (2017). An atlas of human long non-coding RNAs with accurate 5′ ends. Nature *543*, 199–204.

Hormozdiari, F., van de Bunt, M., Segrè, A.V., Li, X., Joo, J.W.J., Bilow, M., Sul, J.H., Sankararaman, S., Pasaniuc, B., and Eskin, E. (2016). Colocalization of GWAS and eQTL Signals Detects Target Genes. Am. J. Hum. Genet. *99*, 1245–1260.

Huber, W., von Heydebreck, A., Sültmann, H., Poustka, A., and Vingron, M. (2002). Variance stabilization applied to microarray data calibration and to the quantification of differential expression. Bioinformatics *18* (*Suppl 1*), S96–S104.

Iyer, M.K., Niknafs, Y.S., Malik, R., Singhal, U., Sahu, A., Hosono, Y., Barrette, T.R., Prensner, J.R., Evans, J.R., Zhao, S., et al. (2015). The landscape of long noncoding RNAs in the human transcriptome. Nat. Genet. *47*, 199–208.

Jiang, S., Cheng, S.-J., Ren, L.-C., Wang, Q., Kang, Y.-J., Ding, Y., Hou, M., Yang, X.-X., Lin, Y., Liang, N., and Gao, G. (2019). An expanded landscape of human long noncoding RNA. Nucleic Acids Res. *47*, 7842–7856.

Karczewski, K.J., Francioli, L.C., Tiao, G., Cummings, B.B., Alföldi, J., Wang, Q., Collins, R.L., Laricchia, K.M., Ganna, A., Birnbaum, D.P., et al.; Genome Aggregation Database Consortium (2020). The mutational constraint spectrum quantified from variation in 141,456 humans. Nature *581*, 434–443.

Keinan, A., and Clark, A.G. (2012). Recent explosive human population growth has resulted in an excess of rare genetic variants. Science *336*, 740–743.

Kerimov, N., Hayhurst, J.D., Peikova, K., Manning, J.R., Walter, P., Kolberg, L., Samoviča, M., Sakthivel, M.P., Kuzmin, I., Trevanion, S.J., et al. (2021). eQTL Catalogue: a compendium of uniformly processed human gene expression and splicing QTLs. bioRxiv. https://doi.org/10.1101/2020.01.29.924266.

Kornienko, A.E., Dotter, C.P., Guenzl, P.M., Gisslinger, H., Gisslinger, B., Cleary, C., Kralovics, R., Pauler, F.M., and Barlow, D.P. (2016). Long non-coding RNAs display higher natural expression variation than protein-coding genes in healthy humans. Genome Biol. *17*, 14.

Kuleshov, M.V., Jones, M.R., Rouillard, A.D., Fernandez, N.F., Duan, Q., Wang, Z., Koplev, S., Jenkins, S.L., Jagodnik, K.M., Lachmann, A., et al. (2016). Enrichr: a comprehensive gene set enrichment analysis web server 2016 update. Nucleic Acids Res. *44* (W1), W90–W97.

Langfelder, P., and Horvath, S. (2008). WGCNA: an R package for weighted correlation network analysis. BMC Bioinformatics *9*, 559.

Langfelder, P., Zhang, B., and Horvath, S. (2008). Defining clusters from a hierarchical cluster tree: the Dynamic Tree Cut package for R. Bioinformatics *24*, 719–720.

Lepik, K., Annilo, T., Kukuškina, V., Kisand, K., Kutalik, Z., Peterson, P., and Peterson, H.; eQTLGen Consortium (2017). C-reactive protein upregulates the whole blood expression of CD59 - an integrative analysis. PLoS Comput. Biol. *13*, e1005766.

Li, W., Notani, D., and Rosenfeld, M.G. (2016). Enhancers as non-coding RNA transcription units: recent insights and future perspectives. Nat. Rev. Genet. *17*, 207–223.

Li, Y.I., Knowles, D.A., Humphrey, J., Barbeira, A.N., Dickinson, S.P., Im, H.K., and Pritchard, J.K. (2018). Annotation-free quantification of RNA splicing using LeafCutter. Nat. Genet. *50*, 151–158.

Liu, S.J., Horlbeck, M.A., Cho, S.W., Birk, H.S., Malatesta, M., He, D., Attenello, F.J., Villalta, J.E., Cho, M.Y., Chen, Y., et al. (2017). CRISPRi-based genome-scale identification of functional long noncoding RNA loci in human cells. Science *355*, aah7111.

Liu, Y., Cao, Z., Wang, Y., Guo, Y., Xu, P., Yuan, P., Liu, Z., He, Y., and Wei, W. (2018). Genome-wide screening for functional long noncoding RNAs in human cells by Cas9 targeting of splice sites. Nat. Biotechnol. *36*, 1203–1210.

Lu, X., Tang, L., Li, K., Zheng, J., Zhao, P., Tao, Y., and Li, L.-X. (2014). Contribution of NKX2-3 polymorphisms to inflammatory bowel diseases: a meta-analysis of 35358 subjects. Sci. Rep. *4*, 3924.

Mattioli, K., Volders, P.-J., Gerhardinger, C., Lee, J.C., Maass, P.G., Melé, M., and Rinn, J.L. (2019). High-throughput functional analysis of lncRNA core promoters elucidates rules governing tissue specificity. Genome Res. *29*, 344–355.

Melé, M., Ferreira, P.G., Reverter, F., DeLuca, D.S., Monlong, J., Sammeth, M., Young, T.R., Goldmann, J.M., Pervouchine, D.D., Sullivan, T.J., et al.; GTEx Consortium (2015). Human genomics. The human transcriptome across tissues and individuals. Science *348*, 660–665.

Melé, M., Mattioli, K., Mallard, W., Shechner, D.M., Gerhardinger, C., and Rinn, J.L. (2017). Chromatin environment, transcriptional regulation, and splicing distinguish lincRNAs and mRNAs. Genome Res. *27*, 27–37.

Mohammadi, P., Castel, S.E., Brown, A.A., and Lappalainen, T. (2017). Quantifying the regulatory effect size of *cis*-acting genetic variation using allelic fold change. Genome Res. *27*, 1872–1884.

Muhvić-Urek, M., Tomac-Stojmenović, M., and Mijandrušić-Sinčić, B. (2016). Oral pathology in inflammatory bowel disease. World J. Gastroenterol. *22*, 5655–5667.

Newman, A.M., Liu, C.L., Green, M.R., Gentles, A.J., Feng, W., Xu, Y., Hoang, C.D., Diehn, M., and Alizadeh, A.A. (2015). Robust enumeration of cell subsets from tissue expression profiles. Nat. Methods *12*, 453–457.

Newman, A.M., Steen, C.B., Liu, C.L., Gentles, A.J., Chaudhuri, A.A., Scherer, F., Khodadoust, M.S., Esfahani, M.S., Luca, B.A., Steiner, D., et al. (2019). Determining cell type abundance and expression from bulk tissues with digital cytometry. Nat. Biotechnol. *37*, 773–782.

Ng, B., White, C.C., Klein, H.-U., Sieberts, S.K., McCabe, C., Patrick, E., Xu, J., Yu, L., Gaiteri, C., Bennett, D.A., et al. (2017). An xQTL map integrates the genetic architecture of the human brain's transcriptome and epigenome. Nat. Neurosci. *20*, 1418–1426.

Novershtern, N., Subramanian, A., Lawton, L.N., Mak, R.H., Haining, W.N., McConkey, M.E., Habib, N., Yosef, N., Chang, C.Y., Shay, T., et al. (2011). Densely interconnected transcriptional circuits control cell states in human hematopoiesis. Cell *144*, 296–309.

Ongen, H., Buil, A., Brown, A.A., Dermitzakis, E.T., and Delaneau, O. (2016). Fast and efficient QTL mapper for thousands of molecular phenotypes. Bioinformatics *32*, 1479–1485.

Pabst, O., Zweigerdt, R., and Arnold, H.H. (1999). Targeted disruption of the homeobox transcription factor Nkx2-3 in mice results in postnatal lethality and abnormal development of small intestine and spleen. Development *126*, 2215–2225.

Pabst, O., Förster, R., Lipp, M., Engel, H., and Arnold, H.-H. (2000). NKX2.3 is required for MAdCAM-1 expression and homing of lymphocytes in spleen and mucosa-associated lymphoid tissue. EMBO J. *19*, 2015–2023.

Panousis, N.I., Gutierrez-Arcelus, M., Dermitzakis, E.T., and Lappalainen, T. (2014). Allelic mapping bias in RNA-sequencing is not a major confounder in eQTL studies. Genome Biol. *15*, 467.

Purcell, S., Neale, B., Todd-Brown, K., Thomas, L., Ferreira, M.A.R., Bender, D., Maller, J., Sklar, P., de Bakker, P.I.W., Daly, M.J., and Sham, P.C. (2007). PLINK: a tool set for whole-genome association and population-based linkage analyses. Am. J. Hum. Genet. *81*, 559–575.

Quek, X.C., Thomson, D.W., Maag, J.L.V., Bartonicek, N., Signal, B., Clark, M.B., Gloss, B.S., and Dinger, M.E. (2015). lncRNAdb v2.0: expanding the reference database for functional long noncoding RNAs. Nucleic Acids Res. *43*, D168–D173.

Quinn, J.J., and Chang, H.Y. (2016). Unique features of long non-coding RNA biogenesis and function. Nat. Rev. Genet. *17*, 47–62.

Regev, A., Teichmann, S.A., Lander, E.S., Amit, I., Benoist, C., Birney, E., Bodenmiller, B., Campbell, P., Carninci, P., Clatworthy, M., et al.; Human Cell Atlas Meeting Participants (2017). The Human Cell Atlas. eLife *6*, e27041.

Roberts, T.C., Morris, K.V., and Wood, M.J.A. (2014). The role of long non-coding RNAs in neurodevelopment, brain function and neurological disease. Philos. Trans. R. Soc. Lond. B Biol. Sci. *369*, 20130507.

Robinson, M.D., McCarthy, D.J., and Smyth, G.K. (2010). edgeR: a Bioconductor package for differential expression analysis of digital gene expression data. Bioinformatics *26*, 139–140.

Robles, E.F., Mena-Varas, M., Barrio, L., Merino-Cortes, S.V., Balogh, P., Du, M.-Q., Akasaka, T., Parker, A., Roa, S., Panizo, C., et al. (2016). Homeobox NKX2-3 promotes marginal-zone lymphomagenesis by activating B-cell receptor signalling and shaping lymphocyte dynamics. Nat. Commun. *7*, 11889.

Stegle, O., Parts, L., Piipari, M., Winn, J., and Durbin, R. (2012). Using probabilistic estimation of expression residuals (PEER) to obtain increased power and interpretability of gene expression analyses. Nat. Protoc. *7*, 500–507.

Storey, J.D., Bass, A.J., Dabney, A., Robinson, D., and Warnes, G. (2020). qvalue: Q-value estimation for false discovery rate control (R package version 2.22.0). http://github.com/jdstorey/qvalue.

Sultan, M., Amstislavskiy, V., Risch, T., Schuette, M., Dökel, S., Ralser, M., Balzereit, D., Lehrach, H., and Yaspo, M.-L. (2014). Influence of RNA extraction methods and library selection schemes on RNA-seq data. BMC Genomics *15*, 675.

Tarlinton, D., Light, A., Metcalf, D., Harvey, R.P., and Robb, L. (2003). Architectural defects in the spleens of Nkx2-3-deficient mice are intrinsic and associated with defects in both B cell maturation and T cell-dependent immune responses. J. Immunol. *170*, 4002–4010.

The Gene Ontology Consortium (2019). The Gene Ontology Resource: 20 years and still GOing strong. Nucleic Acids Res. *47* (D1), D330–D338.

Urbut, S.M., Wang, G., Carbonetto, P., and Stephens, M. (2019). Flexible statistical methods for estimating and testing effects in genomic studies with multiple conditions. Nat. Genet. *51*, 187–195.

van de Geijn, B., McVicker, G., Gilad, Y., and Pritchard, J.K. (2015). WASP: allele-specific software for robust molecular quantitative trait locus discovery. Nat. Methods *12*, 1061–1063.

van Dijk, M., Visser, A., Buabeng, K.M.L., Poutsma, A., van der Schors, R.C., and Oudejans, C.B.M. (2015). Mutations within the LINC-HELLP non-coding RNA differentially bind ribosomal and RNA splicing complexes and negatively affect trophoblast differentiation. Hum. Mol. Genet. *24*, 5475–5485.

Vojkovics, D., Kellermayer, Z., Kajtár, B., Roncador, G., Vincze, Á., and Balogh, P. (2018). Nkx2-3—A Slippery Slope From Development Through Inflammation Toward Hematopoietic Malignancies. Biomark Insights *13*, 1177271918757480.

Võsa, U., Claringbould, A., Westra, H.-J., Bonder, M.J., Deelen, P., Zeng, B., Kirsten, H., Saha, A., Kreuzhuber, R., Kasela, S., et al. (2018). Unraveling the polygenic architecture of complex traits using blood eQTL metaanalysis. bioRxiv. https://doi.org/10.1101/447367.

Walavalkar, K., Saravanan, B., Singh, A.K., Jayani, R.S., Nair, A., Farooq, U., Islam, Z., Soota, D., Mann, R., Shivaprasad, P.V., et al. (2020). A rare variant of African ancestry activates 8q24 lncRNA hub by modulating cancer associated enhancer. Nat. Commun. *11*, 3598.

Wang, K.C., and Chang, H.Y. (2011). Molecular mechanisms of long noncoding RNAs. Mol. Cell *43*, 904–914.

Wapinski, O., and Chang, H.Y. (2011). Long noncoding RNAs and human disease. Trends Cell Biol. *21*, 354–361.

Wright, C.F., FitzPatrick, D.R., and Firth, H.V. (2018). Paediatric genomics: diagnosing rare disease in children. Nat. Rev. Genet. *19*, 253–268.

Xia, B., Yan, Y., Baron, M., Wagner, F., Barkley, D., Chiodin, M., Kim, S.Y., Keefe, D.L., Alukal, J.P., Boeke, J.D., and Yanai, I. (2020). Widespread Transcriptional Scanning in the Testis Modulates Gene Evolution Rates. Cell *180*, 248–262.e21.

Xu, X., Wells, A.B., O'Brien, D.R., Nehorai, A., and Dougherty, J.D. (2014). Cell type-specific expression analysis to identify putative cellular mechanisms for neurogenetic disorders. J. Neurosci. *34*, 1420–1431.

Yanai, I., Benjamin, H., Shmoish, M., Chalifa-Caspi, V., Shklar, M., Ophir, R., Bar-Even, A., Horn-Saban, S., Safran, M., Domany, E., et al. (2005). Genome-wide midrange transcription profiles reveal expression level relationships in human tissue specification. Bioinformatics *21*, 650–659.

Yang, L., Duff, M.O., Graveley, B.R., Carmichael, G.G., and Chen, L.-L. (2011). Genomewide characterization of non-polyadenylated RNAs. Genome Biol. *12*, R16.

Yang, L., Lin, C., Jin, C., Yang, J.C., Tanasa, B., Li, W., Merkurjev, D., Ohgi, K.A., Meng, D., Zhang, J., et al. (2013). lncRNA-dependent mechanisms of androgen-receptor-regulated gene activation programs. Nature *500*, 598–602.

Zerbino, D.R., Wilder, S.P., Johnson, N., Juettemann, T., and Flicek, P.R. (2015). The ensembl regulatory build. Genome Biol. *16*, 56.

Zhu, Z., Zhang, F., Hu, H., Bakshi, A., Robinson, M.R., Powell, J.E., Montgomery, G.W., Goddard, M.E., Wray, N.R., Visscher, P.M., and Yang, J. (2016). Integration of summary data from GWAS and eQTL studies predicts complex trait gene targets. Nat. Genet. *48*, 481–487.

STAR★METHODS

KEY RESOURCES TABLE

REAGENT or RESOURCE	SOURCE	IDENTIFIER
Deposited Data		
GENCODE v26 collapsed single-transcript gene annotation	(GTEx Consortium, 2020)	https://github.com/broadinstitute/gtex-pipeline/tree/master/gene_model
GENCODE v26 comprehensive gene annotation	GENCODE	https://www.gencodegenes.org/human/release_26.html
GTEx WGS and RNA-seq data	(GTEx Consortium, 2020)	dbGaP: phs000424.v8; https://gtexportal.org/home/protectedDataAccess
eQTL data – Buil et al.	(Buil et al., 2015)	https://www.ebi.ac.uk/eqtl/Data_access/
eQTL data – Lepik et al.	(Lepik et al., 2017)	https://www.ebi.ac.uk/eqtl/Data_access/
eQTL data – Võsa et al.	(Võsa et al., 2018)	https://www.eqtlgen.org/
eQTL data – Gutierrez-Arcelus et al.	(Gutierrez-Arcelus et al., 2013)	https://www.ebi.ac.uk/eqtl/Data_access/
eQTL and epigenetic QTL data – Ng et al.	(Ng et al., 2017)	http://mostafavilab.stat.ubc.ca/xqtl/
epigenetic QTL data – Grubert et al.	(Grubert et al., 2015)	https://www.zaugg.embl.de/data-and-tools/distal-chromatin-qtls/
Blood cell expression data	(Novershtern et al., 2011)	GEO: GSE24759
Central nervous system single cell expression data	(Darmanis et al., 2015)	GEO: GSE67835
Mouse Cell Atlas	(Han et al., 2018)	http://bis.zju.edu.cn/MCA/
gnomAD	(Karczewski et al., 2020)	https://gnomad.broadinstitute.org/
UK Biobank GWAS effect size data	Neale lab	http://www.nealelab.is/uk-biobank
1000 Genomes dataset, phase 3	The International Genome Sample Resource	https://www.internationalgenome.org/data
Software and Algorithms		
GTEx *cis*-QTL pipeline	(GTEx Consortium, 2020)	https://zenodo.org/record/3727189
GTEx v8 analysis scripts	(GTEx Consortium, 2020)	https://zenodo.org/record/3930961
STAR v2.5.3a	(Dobin et al., 2013)	https://github.com/alexdobin/STAR
RNA-SeQC v1.1.9	(DeLuca et al., 2012)	https://github.com/getzlab/rnaseqc
optmatch	(Hansen and Klopfer, 2006)	https://github.com/markmfredrickson/optmatch
FastQTL	(Ongen et al., 2016)	https://github.com/francois-a/fastqtl
PEER	(Stegle et al., 2012)	https://github.com/PMBio/peer
edgeR	(Robinson et al., 2010)	https://bioconductor.org/packages/release/bioc/html/edgeR.html
LeafCutter	(Li et al., 2018)	https://davidaknowles.github.io/leafcutter/
mash	(Urbut et al., 2019)	CRAN: mashr
qvalue	(Storey et al., 2020)	https://github.com/StoreyLab/qvalue
vsn	(Huber et al., 2002)	https://www.bioconductor.org/packages/release/bioc/html/vsn.html
WGCNA	(Langfelder and Horvath, 2008)	CRAN: WGCNA
pSI	(Dougherty et al., 2010)	http://genetics.wustl.edu/jdlab/psi_package/
Enrichr	(Kuleshov et al., 2016)	CRAN: enrichR
affy	(Gautier et al., 2004)	https://www.bioconductor.org/packages/release/bioc/html/affy.html
CIBERSORTx	(Newman et al., 2019)	https://cibersortx.stanford.edu/

(*Continued on next page*)

Continued

REAGENT or RESOURCE	SOURCE	IDENTIFIER
GATK ASEReadCounter	(Castel et al., 2015)	https://github.com/broadinstitute/gatk
WASP	(van de Geijn et al., 2015)	https://github.com/bmvdgeijn/WASP
phASER-POP	(Castel et al., 2016)	https://github.com/secastel/phaser
GenomeSTRiP	(Handsaker et al., 2015)	http://software.broadinstitute.org/software/genomestrip/
MELT	(Gardner et al., 2017)	https://melt.igs.umaryland.edu/
Ensembl VEP	Ensembl	https://useast.ensembl.org/info/docs/tools/vep/index.html
GWAS formatting pipeline	This paper	https://github.com/mikegloudemans/gwas-download
SMR & HEIDI	(Zhu et al., 2016)	https://pubmed.ncbi.nlm.nih.gov/27019110/
FINEMAP	(Benner et al., 2016)	http://www.christianbenner.com/
eCAVIAR	(Hormozdiari et al., 2016)	http://genetics.cs.ucla.edu/caviar/
coloc	(Giambartolomei et al., 2014)	CRAN: coloc
Pipeline to run colocalization tools	This paper	https://bitbucket.org/mgloud/production_coloc_pipeline/src/master/
PLINK v1.9	(Purcell et al., 2007)	http://zzz.bwh.harvard.edu/plink/

RESOURCE AVAILABILITY

Lead contact

Further information and requests for resources and reagents should be directed to the Lead Contact, Stephen Montgomery (smontgom@stanford.edu).

Materials availability

Residual GTEx biospecimens have been banked, and are available as a resource for further studies (access can be requested on the GTEx Portal, at https://www.gtexportal.org/home/biobank).

Data and code availability

All GTEx protected data are available at the accession number dbGaP: phs000424.v8. Access to the raw sequence data is now provided through the AnVIL platform (https://gtexportal.org/home/protectedDataAccess). Public-access data, including QTL summary statistics and expression levels, are available on the GTEx Portal, as downloadable files and through multiple data visualizations and browsable tables (https://www.gtexportal.org), as well as in the UCSC and Ensembl browsers.

All components of the single tissue *cis*-QTL pipeline are available at https://github.com/broadinstitute/gtex-pipeline (https://zenodo.org/record/3727189), and analysis scripts are available at https://github.com/broadinstitute/gtex-v8 (https://zenodo.org/record/3930961). From the colocalization analyses, summary statistics and additional input files can be automatically downloaded and formatted consistently using the scripts available at https://github.com/mikegloudemans/gwas-download.

EXPERIMENTAL MODEL AND SUBJECT DETAILS

GTEx subjects

All human donors were deceased, with informed consent obtained via next-of-kin consent for the collection and banking of de-identified tissue samples for scientific research. The research protocol was reviewed by Chesapeake Research Review Inc., Roswell Park Cancer Institute's Office of Research Subject Protection, and the institutional review board of the University of Pennsylvania.

There were 838 donors (557 biological sex male, 281 biological sex female). Donors ranged in age from 20-70, with most enrolled donors being older individuals. For more details on donor characteristics and sample collection, see the GTEx v8 main paper (Data S2) (GTEx Consortium, 2020).

METHOD DETAILS

Biospecimen collection

The biospecimen collection is described in detail in the GTEx v8 main paper (GTEx Consortium, 2020). In brief, whole blood and skin samples were collected from each donor and shipped overnight to the GTEx Laboratory Data Analysis and Coordination Center

(LDACC) at the Broad Institute. These samples were used for DNA genotyping (primarily from whole blood), RNA expression analysis, and culturing and transformation of fibroblast and lymphoblastoid cell lines, respectively. In addition to these samples, two adjacent aliquots were prepared from all other sampled tissues and preserved in PAXgene tissue kits, with ischemic time varying across the different tissue sites. Within each sample pair, one was embedded in paraffin (PFPE) for histopathological review and the second was shipped to the LDACC for processing and molecular analysis. Brains were collected from approximately one-third of the donors, and were shipped on ice to the brain bank at the University of Miami, where eleven brain sub-regions were sampled and flash-frozen. These samples were then shipped to the LDACC for processing and analysis.

A robust quality management program was established and implemented for data management, Standard Operating Procedure (SOP) development, and auditing of collections. Document control software was used to ensure all biospecimen collection sites used current versions of SOPs, and training was conducted prior to implementation of all new procedures. Supporting quality documents were developed to provide consistency and clarity to the program.

Molecular analyte extraction and QC

DNA and RNA extraction and sequencing details are provided in the GTEx v8 main paper (GTEx Consortium, 2020). The same extraction protocols were used for all GTEx samples to avoid introduction of batch effects among samples, which were processed continually throughout the project. To control for variable RNA quality, RNA sequencing was only performed for samples with a RIN score of 5.5 or higher and with at least 500 ng of total RNA. The 49 tissues with $\geq$ 70 genotyped samples that were included in the QTL and other downstream analyses vary in their sample size (n = 73 to 706), ischemic time, and RNA quality (RIN). Additionally, the donor age range varies by tissue; notably the brain samples were collected primarily from older individuals.

QUANTIFICATION AND STATISTICAL ANALYSIS

GTEx data

The v8 freeze of GTEx data includes whole genome sequencing (WGS) data from the whole blood of 838 post-mortem individuals, and RNA-sequencing (RNA-seq) data from 54 tissues. Each tissue has a different sample size for RNA-seq; we confined our analyses to the 49 tissues with N > 70, for a total of 15,201 samples. For more details on data production, see the GTEx v8 main paper (GTEx Consortium, 2020).

Poly(A) selection was performed prior to RNA-seq. RNA-seq libraries prepared by ribosomal RNA depletion and by poly(A) selection quantify similar numbers of lncRNA genes (Sultan et al., 2014). lncRNA genes unique to poly(A) selection tend to be antisense transcripts, whereas lncRNA genes unique to ribosomal RNA depletion tend to be intergenic or intronic lncRNA genes (Sultan et al., 2014). However, in the GTEx data, 96.5% of antisense lncRNA genes were detected in at least one tissue and 94% of intergenic lncRNA genes were detected in at least one tissue; additionally, there were no significant differences in median expression level of lncRNA types across tissues (data not shown). This indicates that poly(A) selection has not drastically skewed quantification of lncRNA types in the GTEx dataset. However, poly(A) selection does prevent the quantification of transcripts that are not polyadenylated, such as enhancer RNAs and excised introns (Li et al., 2016; Yang et al., 2011).

For the tissue-specific expression analyses in this paper, the expression data used were gene-level TPM quantifications produced by RNA-SeQC (DeLuca et al., 2012) following read alignment by STAR (Dobin et al., 2013) to the same GENCODE v26 collapsed single-transcript gene annotation from the GTEx v8 main paper (GTEx Consortium, 2020), which are available on the GTEx Portal.

Defining gene groups

Four gene groups were compared throughout this paper: "total protein-coding genes," "expression-matched protein-coding genes," "total lncRNA genes," and "lncRNA genes with known function." The "total protein-coding genes" group includes any genes with the "protein_coding" biotype in the GTEx GENCODE v26 GTF (19,291 genes). The "total lncRNA genes" group includes any genes with a long non-coding gene biotype ("processed_transcript," "non_coding," "sense_intronic," "sense_overlapping," "antisense," "lincRNA," "macro_lncRNA," "bidirectional_promoter_lncRNA," "3prime_overlapping_ncRNA") in the GTEx GENCODE v26 GTF (14,100 genes).

The "expression-matched protein-coding genes" group were identified through the *pairmatch()* function of the R package optmatch (Hansen and Klopfer, 2006), which takes a treatment group and a larger control reservoir and pairs treatment units to controls in a way that minimizes the sum of the discrepancies between these groups. Expression matching was done separately in each tissue, and matches were limited to the middle 50% of lncRNA genes expressed in that tissue (ranked by median TPM values). Limiting matching to the middle 50% of expressed lncRNA genes kept the group from being so large that sub-optimal matches were made just to ensure that each lncRNA gene had a match. Within each tissue, the treatment group was the middle 50% of expressed lncRNA genes, the larger control reservoir was all expressed protein-coding genes, and *pairmatch()* was run to minimize discrepancies in mean gene expression (TPM). Since expression matching was done within each tissue, the same lncRNA could be matched with different protein-coding genes in different tissues. The expression-matched protein-coding genes across all 49 tissues was a set of 11,178 genes. Whenever possible, the tissue-specific sets of expression-matched protein-coding genes were used, since a pair of genes that have similar expression profiles in one tissue will not necessarily be similar in a different tissue. The only time the entire union set is used at once is the tissue-specificity comparisons in Figure 1F and Figures S1A and S1C.

The "lncRNA genes with known function" are a manually combined set of 954 genes from lncRNAdb (Quek et al., 2015), the HUGO gene nomenclature committee (HGNC, https://www.genenames.org/data/genegroup/#!/group/788), and recent work that identified functional lncRNA genes through splice-site-targeted CRISPR (Liu et al., 2018) and CRISPR interference (Liu et al., 2017) screens; plus 5 genes found in the literature that were not covered in these three sources. Genes from lncRNAdb and the HGNC were only included if they had at least one reference in which direct manipulation of the gene (e.g., knockdown or overexpression) had some effect on cellular phenotype or other genes' expression.

Assessing tissue-specificity of gene expression

A set of tissue-specific lncRNA genes were defined based on having a significantly higher read count than a non-genic region of the same length, as inspired by microarrays and following an approach described by (Chen et al., 2015). First, the coordinates for all non-genic regions were identified by removing all GENCODE v26 exons from the genome, leaving only regions where there was no exonic sequence on either strand. An additional 100 bp was trimmed from both sides of intronic regions, and 1,000 bp from intergenic regions. Then, for each lncRNA gene, a length-matched non-genic region was mapped. This was done one exon at a time: the exon was shifted to the nearest right non-genic region; if it did not fit in that region, it was shifted to the nearest left non-genic region; and so on, bouncing between the next-nearest right and then the next-nearest left region until a non-genic region was found that the exon fit into. In some cases, this sacrificed exon order to select non-genic regions of the same length that were as close to the actual lncRNA gene as possible. Finally, the read counts of the lncRNA genes were compared to the read counts in their non-genic regions, using a paired one-sided Wilcoxon signed rank test (where n = number of samples for a given tissue, ranging from 85 to 803). Genes were called expressed in a tissue if the lncRNA gene count was significantly greater than its matched non-genic region, with a p value < 0.05.

The 49 GTEx tissues have been assigned by GTEx into 28 broad tissue categories (e.g., "Heart, Atrial Appendage" and "Heart, Left Ventricle" tissues are both in the broad tissue category "Heart"). A given gene was considered tissue-specific if the tissues in which it passed the expression test were all a part of the same broad tissue category, and if the median TPM of the genes in all other tissues was < 0.1.

For Figure S1C, Tau scores were used as an additional assessment of tissue-specificity of gene expression (Yanai et al., 2005). Inputs to calculating Tau scores were $\log_2(\text{TPM} + 1)$.

Identifying independent cis-eQTLs and cis-sQTLs by forward stepwise regression-backward selection

The same independent *cis*-eQTLs and *cis*-sQTLs mapped using FastQTL (Ongen et al., 2016) for the main GTEx paper were used in this paper, with expression data normalized by Probabilistic Estimation of Expression Residuals (PEER) (Stegle et al., 2012) and edgeR (Robinson et al., 2010) and splicing quantified by LeafCutter (Li et al., 2018). For full details of the methods used, see the GTEx v8 main paper (GTEx Consortium, 2020). In each tissue, the variants tested were those within 1 Mb of the TSS of each gene and with minor allele frequencies ≥ 0.01, with the minor allele observed in at least 10 samples of that tissue. Independent eQTLs were used for Figures 1B–1D and S1F, and as inputs for the colocalization analyses (see section below). For Figure 1D, the effect sizes of lead eQTLs for protein-coding and lncRNA genes were calculated as allelic fold-change (Mohammadi et al., 2017).

For Figures 1C and 1D, gene groups were compared by Wilcoxon tests, with the n of each gene group equal to the number all lead eQTLs across all tissues for genes in that gene group. Of the main gene groups compared, this ranged from 10,487 for "lncRNAs with known function" to 325,644 for "protein-coding genes."

Identifying tissue-shared cis-eQTLs with mash

The CRAN: mashr (Urbut et al., 2019) results from the main GTEx paper were used (GTEx Consortium, 2020). The output of mash is local false sign rate (LFSR), which is analogous to the false discovery rate, as well as a beta-value effect size. Variant-gene associations with LFSR < 0.05 were considered significant. The mash output data were used in analyses of tissue-specificity of eQTLs, in Figures 1F, 1G, and S1G and Table S2.

Assessing replication of GTEx lncRNA eQTLs

Replication datasets for lncRNA eQTLs were obtained for the following tissues: whole blood (Buil et al., 2015; Lepik et al., 2017; Võsa et al., 2018); EBV-transformed lymphoblastoid cell lines (Buil et al., 2015; Gutierrez-Arcelus et al., 2013); fibroblast cell lines (Gutierrez-Arcelus et al., 2013); brain frontal cortex tissue (Ng et al., 2017); adipose tissue (Buil et al., 2015); and skin (Buil et al., 2015). The eQTL results from Buil et al., Gutierrez-Arcelus et al., and Lepik et al. were obtained from the eQTL Catalogue (Kerimov et al., 2021). For each replication dataset, a set of one variant-gene pair per lncRNA gene was defined, where the variant had the lowest GTEx p value and the variant-gene pair was also tested in the replication dataset. From this set of shared variant-gene pairs, π_1 values were then calculated using the replication dataset's p values for those eQTL tests. The π_1 value is calculated as $\pi_1 = 1 - \pi_0$, and π_0 is the estimate of the proportion of null p values as calculated by R package *qvalue* (Storey et al., 2020). Limitations in this overlap include differences in gene and variant annotation between the studies, expression thresholds for eQTL mapping, and biological differences between groups (for example, GENCORD samples were collected from newborns while GTEx samples were collected from post-mortem adults).

Assessing overlap of GTEx lncRNA eQTLs with other studies' epigenetic QTLs

Datasets for other types of eQTLs (referred to generally as xQTLs) were obtained for the following tissues and QTL types: DNA methylation (DNAm) and H3K9 acetylation (H3K9Ac) QTLs in brain frontal cortex (Ng et al., 2017); and DNase I hypersensitive site (DHS), H3K27 acetylation (H3K27Ac), and H3K4 mono- and tri-methylation (H3K4Me1 and H3K4Me3) QTLs in EBV-transformed lymphoblastoid cell lines (Grubert et al., 2015). For each xQTL dataset, a set of one variant-gene pair per lncRNA gene was defined, where the variant was also tested in the xQTL dataset and the variant was the closest one to the xQTL peak. From this set of variant-gene pairs, π_1 values were then calculated using the xQTL dataset's p values for the marker's QTL tests. The π_1 value is calculated as $\pi_1 = 1 - \pi_0$, and π_0 is the estimate of the proportion of null p values as calculated by R package *qvalue* (Storey et al., 2020). The range size for these xQTL overlaps varied by study and dataset: within 40kb of all histone marker QTLs, and 5kb of the DNAm and DHS QTLs.

Weighted gene correlation network analysis (WGCNA)

Transcript per million (TPM) values quantified by RNASeQC (DeLuca et al., 2012) were normalized on a per tissue basis using the variance-stabilized normalization (VSN) as implemented by the vsn package (Huber et al., 2002). Only genes which met an expression cutoff of at least 0.1 TPM in at least 20% of samples were included. The effects of gene expression batch, Hardy death type, and ischemic time were removed from normalized TPM values in each tissue using an empirical Bayes linear model implemented by the CRAN: *WGCNA* package (Langfelder and Horvath, 2008). Latent factors were not removed from the expression data, because we found that doing so eliminated biological signals necessary for constructing the co-expression networks.

Adjacency matrices were computed using biweight mid-correlation and the default soft-thresholding power of 12. The adjacency matrix was transformed into a topological overlap matrix (TOM) and then subtracted from 1 to create a dissimilarity TOM suitable for hierarchical clustering.

Co-expression modules were identified using the dynamic tree-cutting approach provided by the WGCNA package (Langfelder and Horvath, 2008; Langfelder et al., 2008). The dissimilarity TOM was transformed into a Euclidean distance matrix and a hierarchical clustering tree was created from this matrix using average-linked hierarchical clustering. The hybrid dynamic tree-cutting algorithm was used with a minimum module size of 50 to prevent the creation of very small modules and a deepSplit parameter of 3 to favor more small modules over few large modules. The pamRespectsDendro parameter was set to true, which will force the partitioning around medoids (PAM) step to respect the hierarchical clustering tree when attempting to assign unclustered genes to modules or to merge very similar modules. This is more conservative than setting pamRespectsDendro to false and leads to more genes remaining unclustered.

Eigengenes were computed from the first principal component of the expression values of the genes assigned to each module. Modules whose eigengenes had a biweight mid-correlation greater than 0.8 were merged using the mergeCloseModules function to reduce the number of highly correlated modules. Module membership was estimated as the biweight midcorrelation between each gene and its module eigengene. Scaled intramodular connectivity (k_{in}) was computed from intramodular connectivity for each gene by dividing its intramodular connectivity by the largest intramodular connectivity value in that module (scaled k_{in} range = 0 to 1).

We observed that the number of co-expression modules defined for each tissue ranged from 8 (in cultured fibroblast cells) to 78 (in ovary), with the number of identified modules unrelated to the sample size of the tissue (Figure S2A). Of these modules, 18% (in ovary) to 81% (in stomach) were annotated (Figure S2B). This percentage was related to both the number of modules in a tissue, and the possible cell type gene sets established for that tissue. For most tissues, just over half of lncRNA genes met the expression requirements to be included in the co-expression networks (median included lncRNA genes across tissues = 53%; see Figure 2A). The proportion of included genes was higher for lncRNA genes with known functions (median = 71%).

Co-expression network module annotation via gene set enrichment

In large modules, gene set enrichment was limited to the top 500 genes as ranked by module membership. Enrichments for both cell compartments and cell types were assessed.

For cell compartment gene sets, only four terms were tested: nucleolus (GO:0005730), mitochondrion (GO:0005739), mitochondrial inner membrane (GO:0005743), and cytosolic ribosome (GO:0022626). This was because our aim was to eliminate spurious cell type enrichment driven by cell compartment rather than cell types. Enrichment was computed using the hypergeometric overlap test between the genes in the module and list of cell compartment genes provided by GO Cellular Compartment (Ashburner et al., 2000; The Gene Ontology Consortium, 2019). Enrichment p values were adjusted for the number of modules and the number of terms in each tissue network using Bonferroni correction.

Enrichment for cell types across 20 tissues were computed using cell type specificity index (SI) values estimated by the pSI package (Dougherty et al., 2010; Xu et al., 2014) in the datasets described in the STAR Methods section "Cell type annotation sources." For each module, a linear model was fitted with a dummy variable indicating membership in the module or (or the top 500 genes in the module for large modules) as the predictor, and the SI values as the outcome. Only genes found in both the network and annotation were used in the model. Because a lower SI value indicates a higher cell type specificity, only models with a negative coefficient were considered a valid enrichment. All enrichment p values were Bonferroni-corrected for the number of modules and the number of cell types in each dataset.

Final annotations were decided by combining the cell compartment and cell type annotations. Modules with strong enrichment for mitochondria or ribosomes were annotated for those compartments over cell types. Cell types present in multiple tissues from the annotation sources (such as resident immune cells, epithelial cells, or stromal cells) were accepted as annotations if there was agreement from multiple tissues. Tissue-specific cell types were only used as a module annotation if they were in the appropriate tissue. For tissues without a direct analog in the annotation sources, cell type annotations were assigned by looking across all available tissues in the annotation sources. If a module was annotated for a mix of cell types, it was submitted to Enrichr (Chen et al., 2013; Kuleshov et al., 2016) to assist in identifying other pathways. If this did not clarify the annotation, the module was called "unannotated."

Cell type annotation sources

Blood cell type-specific expression data was obtained from a published dataset (GSE24759) (Novershtern et al., 2011). Raw CEL files were imported and normalized with RMA using the affy package (Gautier et al., 2004). Progenitor cells and cell types with a small number of samples were excluded, and some cell subtypes were aggregated. The final dataset used to estimate specificity index values was the averaged expression values for the samples corresponding to the following 13 cell types: naive CD4+ T cell, memory CD4+ T cell, naive CD8+ T cell, memory CD8+ T cell, naive B cell, mature B cell, mature NK cell, monocyte, myeloid dendritic cell, granulocyte (neutrophil), basophil, eosinophil, and megakaryocyte.

Cell type-specific expression for the central nervous system was obtained from a published single-cell RNA dataset (Darmanis et al., 2015). Fetal cell types were excluded and log counts were averaged for estimating specificity index values for six cell types: neuron, astrocyte, oligodendrocyte, oligodendrocyte progenitor cell (OPC), microglia and endothelial cell.

The remaining cell type specific expression data was obtained from the Mouse Cell Atlas (Han et al., 2018). Counts data was downloaded from Mouse Cell Atlas website (http://bis.zju.edu.cn/MCA/) and log normalized. All adult tissues with a matching tissue in GTEx were used except peripheral blood and brain and neonatal heart was also included because no adult heart sample was available. Some cell subtypes were collapsed, and averaged cell type matrices were computed for 18 tissues: heart, kidney, liver, lung, mammary gland (involution), mammary gland (lactation), mammary gland (pregnancy), mammary gland (virgin), muscle, ovary, skin, pancreas, prostate, small intestine, spleen, stomach, testis, and uterus.

Identifying lncRNA genes with high confidence cell type annotations in brain and blood tissues

For lncRNA genes assigned to cell type modules in brain and blood tissues, we assessed which of these genes' annotation was further supported by correlation of the gene's expression with that cell type's estimated proportion. First, we estimated cell composition in all GTEx samples from brain tissues and whole blood using CIBERSORTx (Newman et al., 2019). The LM22 blood cell type reference (Newman et al., 2015) provided by CIBERSORTx was used for estimating blood cell composition, while a published single cell brain dataset (Darmanis et al., 2015) was used as a reference from brain regions. Default settings were used for creating the signature matrix for the brain reference and imputing cell fractions, with the recommended B-mode batch correction being used to normalize GTEx samples to the reference datasets.

Then, within each GTEx brain tissue and within GTEx whole blood, we performed a Pearson correlation test between each lncRNA gene's expression and each cell type's estimated proportion. The input gene expression data was log2(read counts + 1). The n for each test was the number of samples for the given brain or blood tissue, ranging from 139 to 755. Benjamini-Hochberg multiple test correction (Benjamini and Hochberg, 1995) was done across all tests within each tissue, and a significant correlation was an adjusted p value < 0.05.

Finally, we identified which lncRNA genes showed agreement in their WGCNA module annotations, and their correlation with CIBERSORTx-estimated cell type proportion. For brain, since there are ten different brain tissue types sampled in GTEx, we required agreement of WGCNA and CIBERSORTx-based annotation in multiple brain tissues. Specifically, to have high confidence cell type annotation, a lncRNA gene had to be significantly correlated with the same cell type in at least four brain tissues, and this correlation had to be in the same direction (all positive or all negative). In at least one of these brain tissues, the gene must be assigned to a WGCNA module annotated as that cell type. The gene must also not be assigned to a WGCNA module annotated as any other cell type in the other brain tissues (although a cell compartment annotation, such as "mitochondria," would be acceptable). For blood, since there is only one tissue type (whole blood), we could not be as stringent as we were with gene annotations in brain tissue. Instead, a lncRNA gene had high confidence cell type annotation if it was significantly correlated with the same cell type to which it was annotated using WGCNA. The cell types estimated by CIBERSORTx for blood were more specific than the annotation categories used in WGCNA, so the two approaches just had to annotate the gene to similar cell types to be considered in agreement. For example, significant correlation with CIBERSORTx-estimated proportion of "T cells, CD4 naive" and WGCNA assignment to "T cell" module in whole blood was considered an agreement.

Allele-specific expression (ASE)

Autosomal ASE data were produced using GATK ASEReadCounter tool (Castel et al., 2015) and the WASP filtering strategy (van de Geijn et al., 2015) to remove read mapping bias, as described in the GTEx main paper (GTEx Consortium, 2020) and the GTEx ASE companion paper (Castel et al., 2020). ASE sites were removed if they were in low-mappability regions (75-mer mappability with leq2 mismatches < 1), showed mapping bias in simulation (Panousis et al., 2014), or had no more reads supporting two alleles than would

be expecting from sequencing noise alone, indicating potential genotyping error (FDR < 1%, see Castel et al., 2015, for description of test).

We used phASER-POP (Castel et al., 2016) to obtain p values for regulatory effects of the unique set of top eQTL and sQTL in every gene in every tissue in GTEx. Inputs for phASER-POP were the WASP-corrected haplotype expression matrix, the read-backed phased VCF generated for the GTEx ASE companion paper (Castel et al., 2020), and gene-variant pairs corresponding to the top eQTL and sQTL for every gene in every tissue obtained from the eQTL and sQTL summary statistics generated for the GTEX main paper (GTEx Consortium, 2020). We used the default setting of 10,000 bootstrap samples for estimating allelic fold change (aFC) p values. Although this approach allows us to score and assign significance to the level of ASE as mediated by a given variant, a limitation of it was that only genes with either an eQTL or sQTL could be analyzed.

Since the aFC p values were obtained via bootstrapping, some variants had p values of 0. These values were changed to $1x10^{-4}$ (the equivalent to one bootstrap sample supporting the null) so that they could be converted to finite Z scores. Variant-level Z scores were calculated from aFC p values, and averaged over the variants in each gene to produce gene-level Z scores. For a given gene, its mean neighbor Z score was calculated by averaging the gene-level Z scores for all genes within ± 500kb of the gene.

We defined ASE-sharing as all occurrences where a gene-level Z score and its corresponding mean neighbor Z score was greater than 3. We computed gene biotype enrichment for ASE-sharing using Fisher's test, comparing the number of genes showing ASE-sharing in intergenic lncRNA genes and antisense lncRNA genes to protein coding genes, relative to the total number of genes in each class. The numbers of genes in each comparison are provided in Figure 3B.

ASE data can be noisy, since differences in read coverage along a gene results in variation in ASE measurements across the informative variants within that gene. Although we have mitigated this by aggregating ASE scores across the variants in a gene and by using stringent Z score thresholds to select a robust set of genes with high ASE, one might want to prioritize genes with low variation in their ASE measurements. In addition to reporting the mean Z score for a gene and its neighboring genes, we also provide the coefficients of variation for these two Z scores (Table S4).

Multi-tissue gene expression outlier discovery

We subset expression data in each tissue to genes with 6 reads and TPM > 0.1 in at least 20% of individuals. Within each tissue, the TPM values were log transformed, (log2(TPM + 2)), and scaled across individuals for each gene. We regressed out the effects of the first three genotype principal components, sex, and hidden factors discovered via PEER (Stegle et al., 2012), the number of which depends on sample size for that tissue and was consistent with the GTEx eQTL discovery pipeline (GTEx Consortium, 2020): for tissues with less than 150 samples, we removed 15 PEER factors; less than 250 samples, 30 factors; less than 350, 45 factors; and 60 for the remaining tissues. We additionally corrected for the genotype of the strongest *cis*-eQTL per gene per tissue to magnify rare variant effects, which has been shown to improve nearby rare variant enrichments (Ferraro et al., 2020). We then re-scaled expression values across individuals within each gene to generate corrected Z scores per individual per gene per tissue.

For each gene-individual pair, if that individual has expression measurements in at least five tissues, we calculate a median Z score for that gene. We define outlier individuals as those with a |median Z score| greater than 2, and non-outliers as all other individuals for the same set of genes. We removed as global outliers 39 individuals for whom the proportion of tested genes were outliers at a threshold of |median Z score| > 3 exceeded 1.5 times the interquartile range of the distribution of proportion outlier genes per individual. For outlier analysis, we include all autosomal intergenic lncRNA and protein-coding genes. We focused much of our outlier analysis on widely-expressed intergenic lncRNA genes, which were genes with read counts significantly greater than their length-matched non-genic regions in all tissues.

To assess variant enrichments, we subset to 714 individuals who self-report with European ancestry, as allele frequencies are less comparable between continental populations. We retain all SNPs and indels that pass quality control in the GTEx *VCF*. Structural variants were called in a subset of these individuals as in Chiang et al. (2017) with GenomeSTRiP GSCNQUAL (Handsaker et al., 2015) set to limit the false discovery rate (FDR) for each variant type. GenomeSTRiP's IntensityRankSumAnnotator was used to evaluate FDR based on available Illumna Human Omni 5M gene expression array data. GSCNQUAL was limited to ≥ 1 for GenomeSTRiP deletions and ≥ 8 for multi-allelic copy number variants, corresponding to an FDR of 10%. The GSCNQUAL cutoff for GenomeSTRiP duplications was set at ≥ 17, the point where the FDR plateaued at 15.1% and did not fluctuate more than ± 1% for over 50 steps in increasing GSCNQUAL score. Additionally, the Mobile Element Locator Tool (MELT) (Gardner et al., 2017) version 2.1.4 was run using MELT-SPLIT to identify ALU, SVA, and LINE1 insertions into the test genomes. MELT calls that were categorized as "PASS" in the VCF info field, had an ASSESS score ≥ 3, and SR count ≥ 3 were retained.

We define rare variants as those with < 1% frequency in GTEx, and for SNPs and indels, also < 1% frequency in non-Finnish Europeans from the gnomAD database (Karczewski et al., 2020). Remaining bins are defined by GTEx allele frequencies. We calculate relative risk as the proportion of outlier individuals with a variant of a given frequency within 10kb of the outlier gene or in the gene body over the proportion of non-outlier individuals with a variant of a given frequency within 10kb of or in the gene body of the same set of genes. Variant categories were annotated using Ensembl VEP (version 88) and each gene-individual pair was assigned to the most enriched variant category, regardless of the number of nearby rare variants.

Data to assess the GWAS effect size for body-mass index in outlier-associated rare variants was obtained from http://www.nealelab.is/uk-biobank. We first identified all intergenic lncRNA gene expression outliers with a nearby rare variant that was not observed in any control individuals (those with |median Z score| < 1), and that had no protein-coding gene expression outliers within

1Mb. At an outlier threshold of |median Z score| $\geq$ 2, this produced an outlier pool of 44 rare variants for 26 outlier intergenic lncRNA genes. We next identified a non-outlier pool of 3,173 rare variants from control individuals with |median Z score| < 1 for these same genes. We then performed 1,000 permutations of randomly selecting one outlier variant and one non-outlier variant from each gene, and calculating the mean GWAS effect sizes in the two groups; these produce the distributions shown in Figure 4D and compared by Wilcoxon test.

GWAS sources and data preparation for colocalization analysis

We downloaded publicly available full-genome summary statistics from 176 papers (Table S6). We focused on studies of diseases and traits related to neurological and immune function, since these are contexts in which smaller scale lncRNA studies have found these genes to have compelling roles (Heward and Lindsay, 2014; Roberts et al., 2014). We re-formatted the GWAS statistics into a standardized tab-separated format for compatibility with our colocalization pipeline tools, and indexed them using the bgzip and tabix command line utilities using the above Github repository.

Selecting colocalization tests

To restrict the total number of intended colocalization tests to a computationally tractable number, we first performed a naive overlap test of the GWAS summary statistics and the GTEx sQTL and eQTL association summary statistics. For each GWAS, we selected all SNPs in any of our selected GWAS with a nominal association p value < 1e-12, chosen as the least stringent threshold that was computationally tractable. We additionally required that selected SNPs be at least 1 Mb apart from all SNPs already selected from the same GWAS, to ensure independence of effects and different loci. For every selected GWAS SNP, we identified all eQTL or sQTL features (gene expression and splice junction usage, respectively) that had a QTL association p value < 1e-5 at any SNP positioned within 10kb of the most significant GWAS SNP at the locus. We make no quantitative claims about the significance of these naive overlaps, as many such overlaps could be expected by chance; these merely formed the set of loci to test for colocalization in subsequent steps.

The result from this step was a list of 1,153 unique lead SNPs from 176 GWAS, and 49 GTEx QTL tissues with a total of 13,804 individual QTL features. Each site to be tested for colocalization consisted of a SNP / GWAS trait / QTL feature / QTL tissue combination.

We then tested every resulting pair of GWAS locus and QTL feature in our set, using three gene prioritization or colocalization methods: SMR+HEIDI (Zhu et al., 2016), FINEMAP+eCAVIAR (Benner et al., 2016; Hormozdiari et al., 2016) and CRAN: *coloc* (Giambartolomei et al., 2014). For each of these GWAS-QTL pairs, we then narrowed our summary statistics to the set of the SNPs tested for association with both the given GWAS trait and the given QTL trait, and removed all sites containing less than 50 SNPs after this filter.

Colocalization approaches: SMR + HEIDI

Summary data-based Mendelian Randomization (SMR) tests for association between a feature and trait using variant-feature and variant-trait association statistics in a two-sample Mendelian Randomization framework (Zhu et al., 2016). The HEIDI test, typically applied to significant SMR results, eliminates cases where the association is driven by linkage or proximity of independent causal variants rather than a shared causal variant.

We ran SMR using the default parameter settings to obtain an SMR p value for each locus and a HEIDI p value at each locus. For the remainder of the tested loci, we report the Bonferroni-adjusted SMR p values. Significant colocalizations were those with the number of overlapping GWAS/eQTL SNPs within the tested window > 50, an SMR Bonferroni-adjusted p value < 1e-05, and that did not show evidence of heterogeneity of estimated effects (i.e., did not show evidence of linkage) using the HEIDI test (HEIDI p value $\geq$ 0.05). SMR+HEIDI colocalization scores were reported as $-\log_{10}$(SMR adjusted p value).

Colocalization approaches: FINEMAP

FINEMAP is a variant association fine-mapping tool that identifies the set of causal variants with a predefined probability for a given GWAS or QTL (Benner et al., 2016). eCAVIAR then can be used to combine the FINEMAP outputs for a given GWAS and a given QTL, and compute the probability of their colocalization (Hormozdiari et al., 2016).

Using the full 1000 Genomes dataset from phase 3 (2,504 individuals) as a reference population (Auton et al., 2015), we estimated LD between all of these SNP pairs using PLINK (Purcell et al., 2007). We then ran FINEMAP independently on the GWAS and the QTL summary stats to obtain posterior probabilities of causality for each of the remaining SNPs. These probabilities were then combined to compute a colocalization posterior probability (CLPP) using the formula described in the eCAVIAR method. These are the values we report in the paper, with significant colocalizations having CLPP $\geq$ 0.02, with the number of overlapping GWAS/eQTL SNPs within the tested window > 50. We ran FINEMAP using the default settings and assumed the existence of exactly one causal variant in both the GWAS and the QTL summary stats, in accordance with common practice. FINEMAP colocalization scores were the CLPP scores.

Colocalization approaches: coloc

coloc is a Bayesian approach that estimates the support for all possible hypotheses involving a given GWAS and a given QTL: H0, neither trait has a genetic association in the region; H1: only the GWAS has a genetic association in the region; H2: only the QTL has a

genetic association in the region; H3: both the GWAS and QTL are associated, but with different causal variants; H4: both the GWAS and QTL are associated and share a single causal variant (Giambartolomei et al., 2014).

At a given locus, we estimated the allele frequencies for each variant appearing in both the GWAS and the QTL summary statistics. The allele frequencies were supplied along with the p values as inputs to the *coloc* package (using the coloc.abf function to estimate posterior probability of colocalization). The default priors were used for the function. The summary statistics we reported for each locus are the PP4 value, which denotes the probability that both the eQTL and the GWAS have a variant at the locus with non-zero effect, and that they are the same causal variant. Significant colocalizations were those that had a PP4 $\geq$ 0.80, with the number of overlapping GWAS/eQTL SNPs within the tested window > 50. *coloc* colocalization scores were the PP4 values.

Integrating and interpreting the colocalization results

The GTEx variant annotation, which was used when examining the 95% credible sets of variants from FINEMAP colocalizations, was compiled from Ensembl's Variant Effect Predictor and Loss-Of-Function Transcript Effect Estimator (VEP v85), and the Ensembl Regulatory Build (GTEx Consortium, 2020; Zerbino et al., 2015).

For the neighboring genes assessment, each significant lncRNA gene colocalization score was compared to the colocalization scores for the same GWAS, GTEx tissue, and colocalization approach of all protein-coding genes 500kb up or downstream of the gene. In addition to categorically evaluating whether the lncRNA gene's colocalization score was the greatest in its 1Mb range, we also calculated a metric comparing a lncRNA gene's score to its adjacent genes. First, the score differences were calculated for each colocalization event: this was (gene of interest's colocalization score - greatest adjacent protein-coding gene's colocalization score). Then, since each colocalization approach has different scoring scales, these score differences were converted into ranks. All colocalization events with a score difference of 0 (i.e., the gene of interest had the exact same colocalization score as a nearby protein-coding gene) were given the same rank. These ranks were then scaled by the total number of significant colocalizations discovered by that approach. Finally, each colocalization event was discovered by anywhere from one to three different approaches: we calculated an aggregated score by taking the mean of the scaled rank values for each approach that discovered this colocalization (GWAS-feature-tissue combination).

Supplemental figures

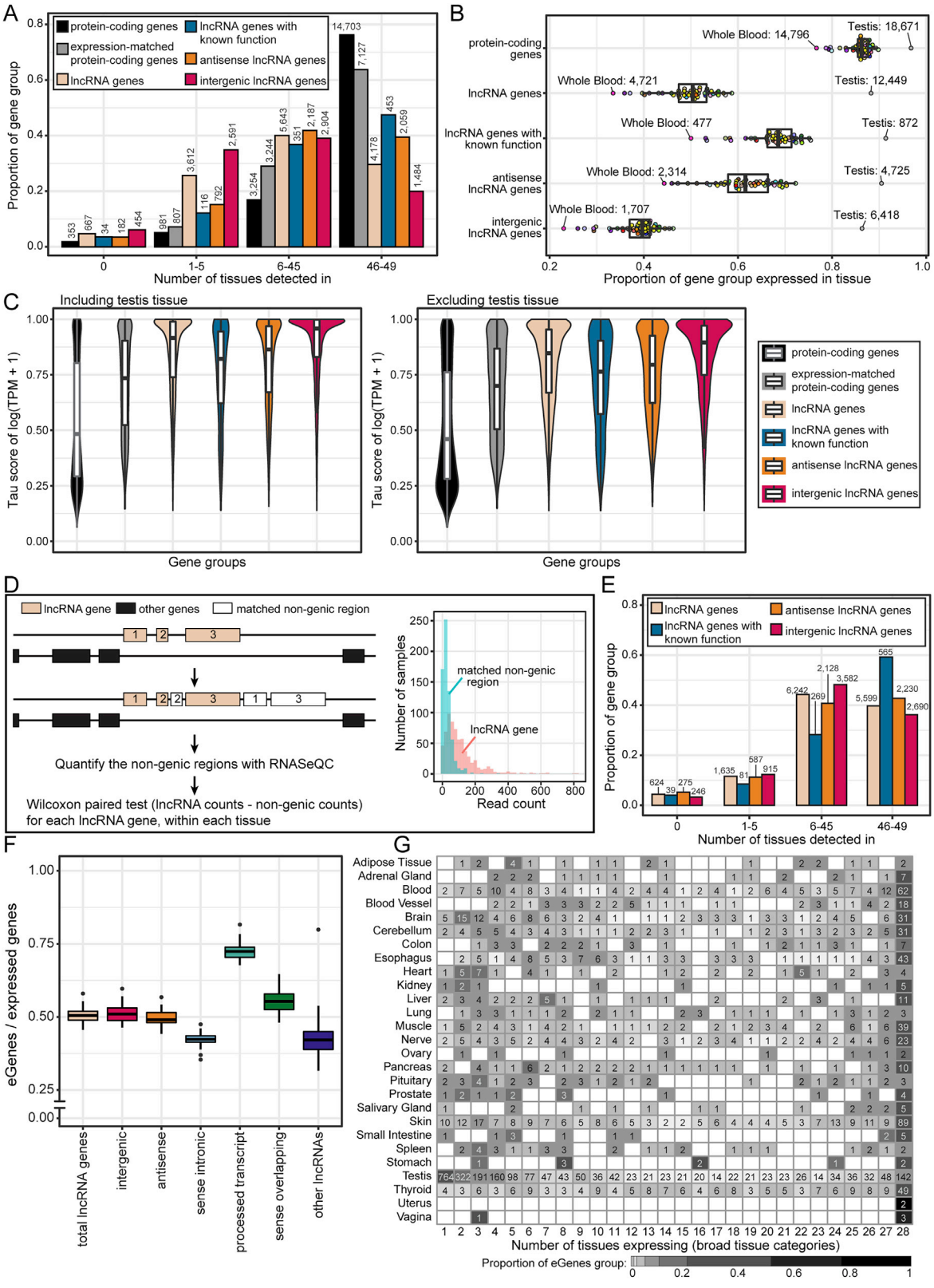

(legend on next page)

Figure S1. Gene expression and eQTL patterns of lncRNA and protein-coding genes, related to Figure 1 and Tables S1 and S2

(A) The number of tissues expressing each gene type, at an expression threshold of TPM > 0.1 in > 20% of samples. Bar labels show the number of genes.

(B) The proportion of each gene group expressed in each tissue, at a threshold of TPM > 0.1 in > 20% of samples. Data points reflect the proportion of a gene group expressed in a given tissue, with point color indicating the tissue. The overlaying boxplots represent the medians with first and third quartiles as boxes, and whiskers extending to 1.5 times the interquartile range. The most extreme values are labeled with the tissue name and number of genes expressed.

(C) Tissue-specificity of gene expression based on Tau scores. Since the testis tissue has such a distinctive gene expression profile and drove much of the observed tissue-specificity, Tau scores were calculated both including expression values from the testis tissue (*left*) and excluding the testis tissue (*right*). The boxplots represent the medians with first and third quartiles as boxes, and whiskers extending to 1.5 times the interquartile range.

(D) Illustration of how lncRNA genes were called expressed relative to background read counts. The cartoon (*left*) shows how matched non-genic regions were found for lncRNA genes. Note that non-genic regions could be intergenic or intronic, as long as they did not overlap with a gene on either strand; and that proximity to the original lncRNA gene was prioritized over maintaining "exon" order. The read count histogram (*right*) shows an example of a lncRNA gene with greater expression than its matched non-genic region.

(E) The number of tissues expressing each lncRNA gene type, based on testing read counts between the lncRNA genes and their matched non-genic regions. Bar labels show the number of genes.

(F) Proportion of expressed lncRNA genes that were also eGenes, separated by lncRNA gene type. Boxplots reflect the range of proportions across the 49 GTEx tissues, representing the medians with first and third quartiles as boxes, and whiskers extending to 1.5 times the interquartile range.

(G) For each set of broad tissue-specific eGenes (rows of heatmap), the shading indicates the proportion that were expressed in a given number of tissues (columns of heatmap) at a threshold of $\geq$ 0.1 TPM in > 20% of samples. Both protein-coding and lncRNA tissue-specific eGenes are included in this heatmap. The labels indicate many of the tissue-specific eGenes were expressed in the corresponding number of tissues. There is no row for Breast tissue because it had no tissue-specific eGenes.

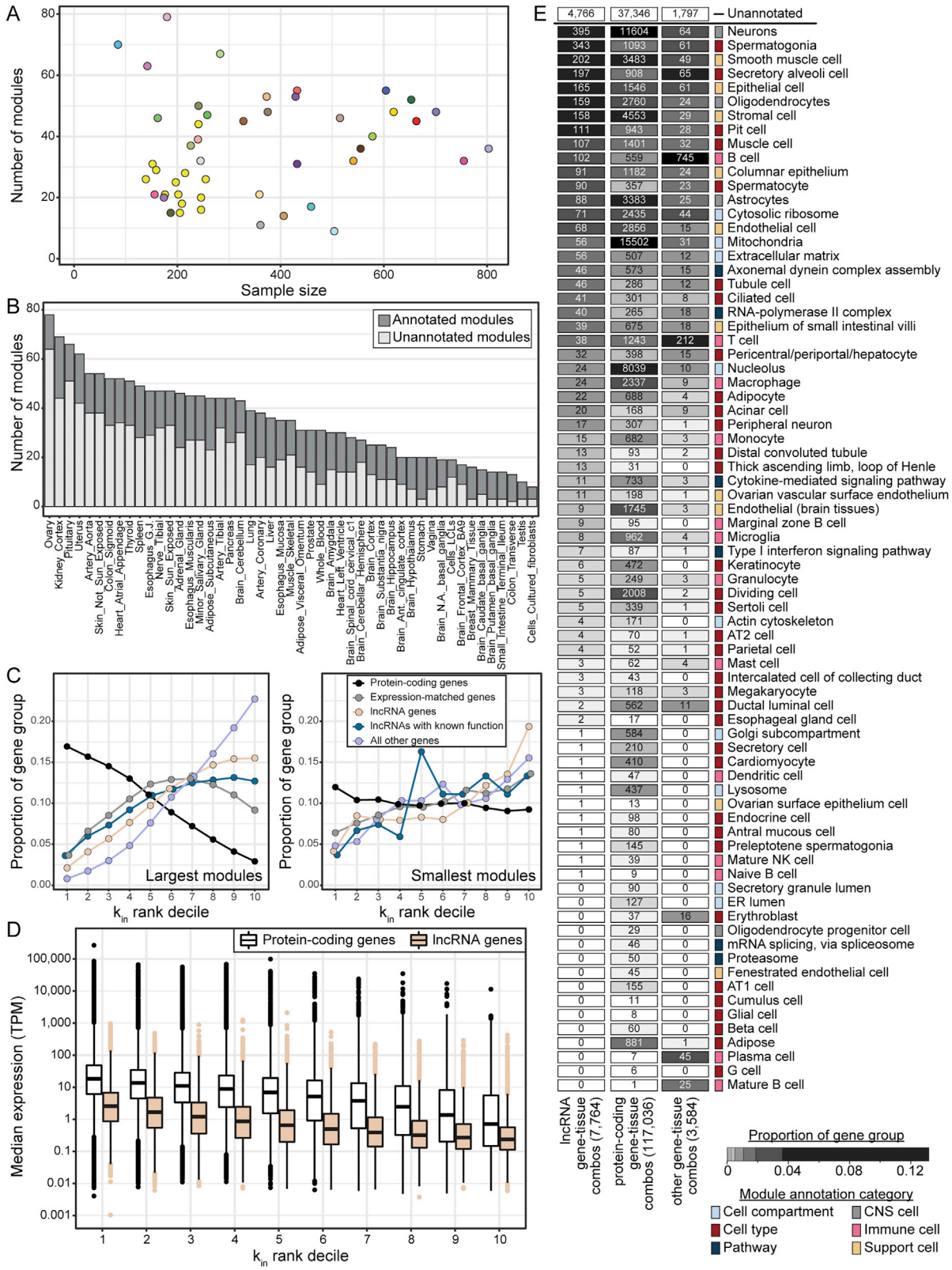

(legend on next page)

Figure S2. Connecting genes through weighted gene co-expression network analysis (WGCNA), related to Figure 2 and Data S1

(A) The number of co-expression modules identified in each tissue was not related to the sample size of the tissue. The fill color of points indicates tissue.

(B) The number of modules with a cell type or cell compartment annotation versus the number that were unannotated in each tissue. There was also one module of unclustered genes per tissue, which is not depicted.

(C) Proportion of gene groups binned by intra-modular connectivity (k_{in}) ranking, in the largest modules (*left*; 1,876-16,840 genes) and smallest modules (*right*; 50-72 genes). The most highly connected genes within their module are in the first k_{in} rank decile, and the least connected genes within their module are in the tenth k_{in} rank decile.

(D) Median expression level (TPM) of protein-coding and lncRNA genes binned by their k_{in} rank decile. On average, gene expression was higher in genes with greater intra-modular connectivity. Data represented are the medians with first and third quartiles as boxes, and whiskers extending to 1.5 times the inter-quartile range.

(E) Module annotations of the genes in the top k_{in} rank decile of their modules. The box fill reflects the proportion of genes assigned to a module with that annotation. Since genes were assigned to modules in multiple tissues, the labels reflect gene-tissue combinations, not individual genes.

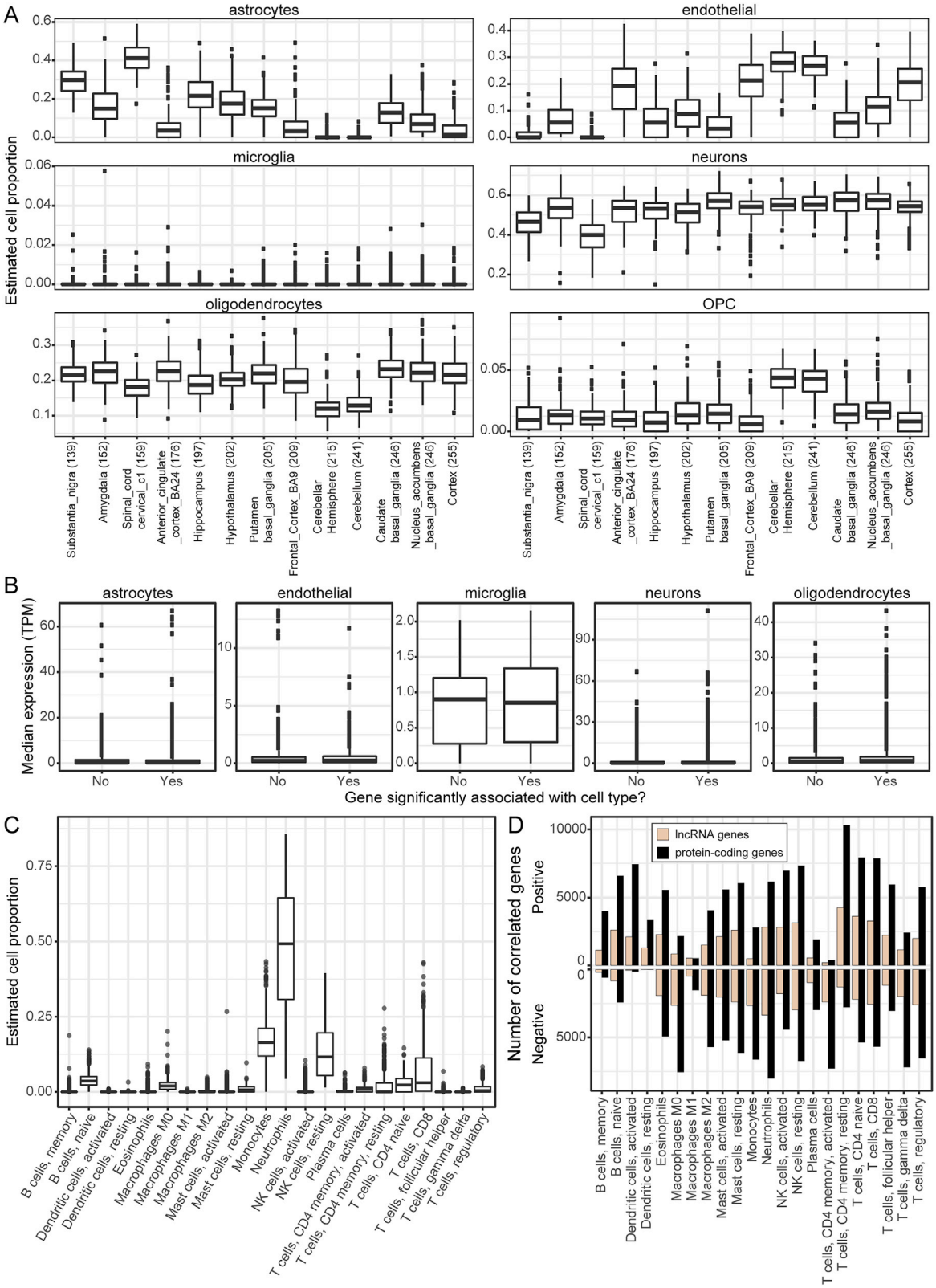

(legend on next page)

Figure S3. Identifying lncRNA genes with high-confidence cell-type annotation in blood and brain tissues using CIBERSORTx, related to Figure 2C and Table S3

(A) Estimated cell proportions of the six different cell types calculated by CIBERSORTx (the panels of the plot) in each of the GTEx brain tissues (x axis).

(B) Median TPM of lncRNA genes across brain tissues, based on whether their expression was significantly correlated with the CIBERSORTx estimated proportion of a certain cell type (and also coincided with WGCNA-based module annotation in that brain tissue). In all boxplots, the data represented are the medians with first and third quartiles as boxes, and whiskers extending to 1.5 times the interquartile range.

(C) Estimated cell proportions of the different blood cell types calculated by CIBERSORTx in blood. The data represented are the medians with first and third quartiles as boxes, and whiskers extending to 1.5 times the interquartile range.

(D) Number of genes correlated with a given cell type proportion, as estimated by CIBERSORTx.

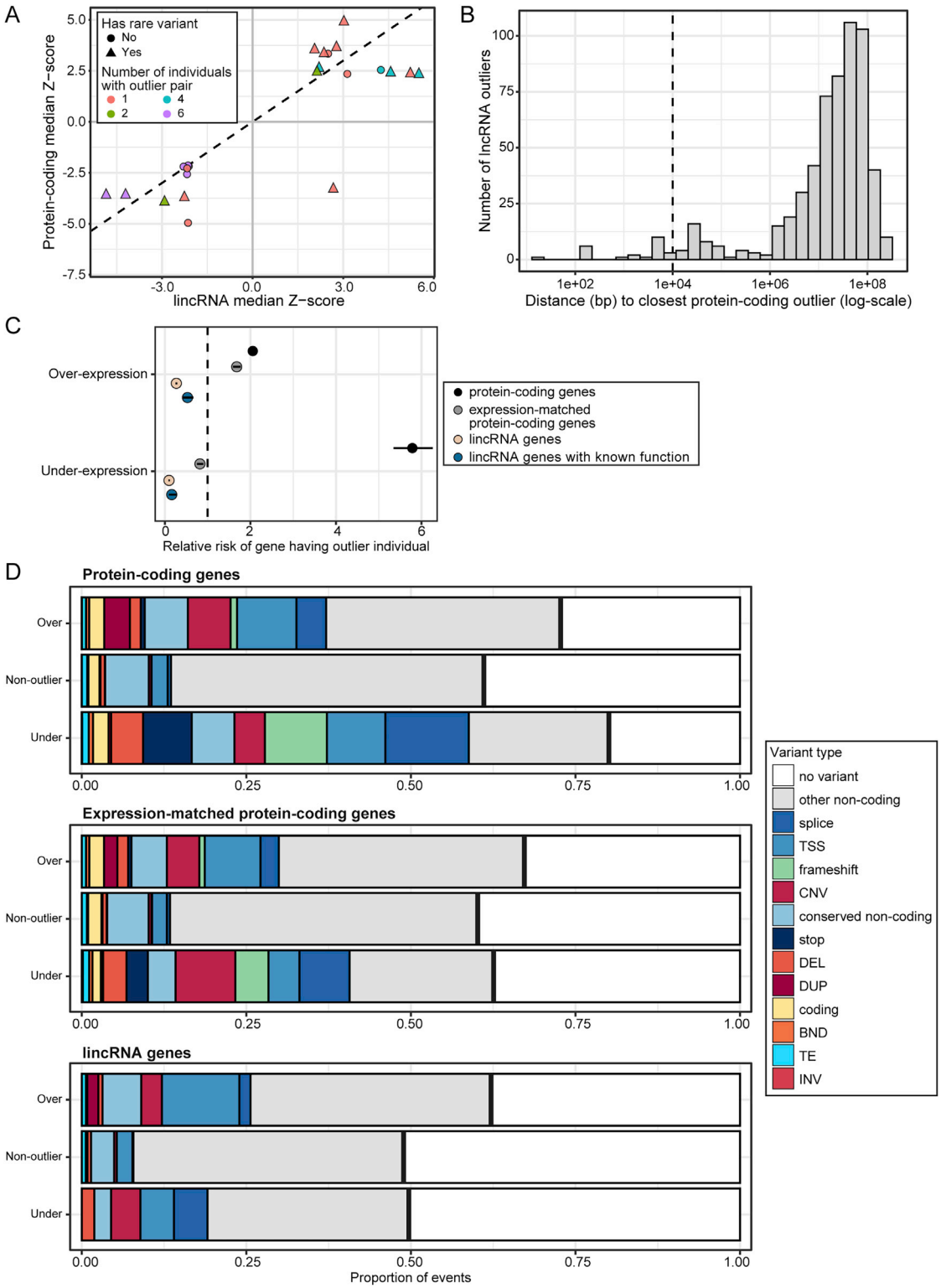

Figure S4. Outliers in intergenic lncRNA gene expression, related to Figure 4 and Table S5

(A) Summary of lncRNA/protein-coding gene pairs that were within 10kb of each other and both outliers in the same individual.

(B) The distance between intergenic lncRNA genes and protein-coding genes that were called multi-tissue outliers in the same individual and were on the same chromosome. The dashed line indicates the threshold of 10kb for the lncRNA/protein-coding gene outlier pairs.

(legend continued on next page)

(C) Enrichment of outlier events in specific gene groups relative to all genes. Data represented are the relative risk ratios, with bars showing the 95% confidence interval.
(D) Presence of rare variants (MAF < 1%) within 10kb of the outlier gene based on outlier status. The bold line separates outlier events with some nearby rare variant from those with no nearby rare variant (white fill).
lincRNA = intergenic lncRNA, TSS = transcription start site, TE = transposable element insertion, BND = breakend, DEL = deletion, CNV = copy number variation, DUP = duplication, INV = inversion.

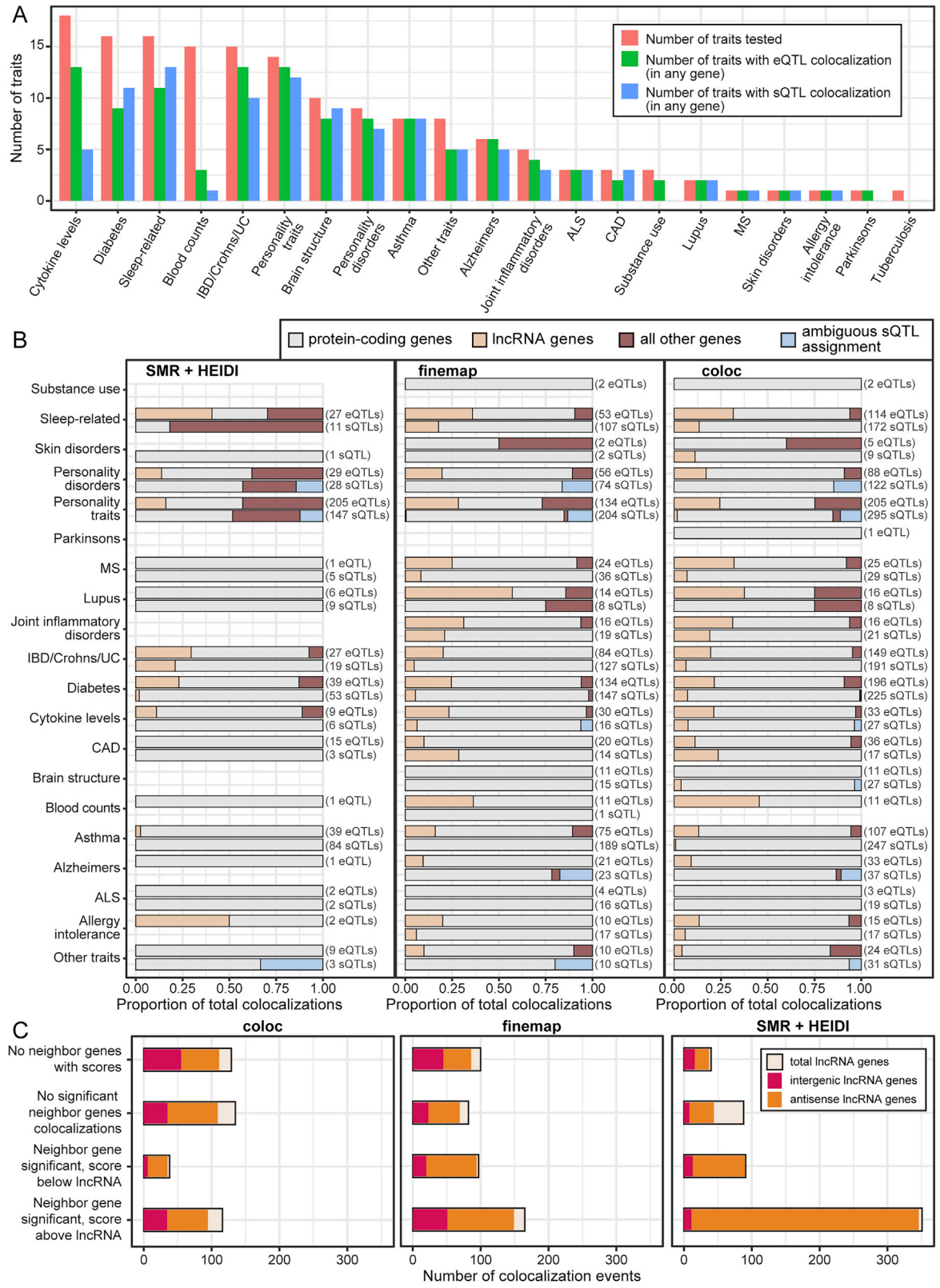

(legend on next page)

Figure S5. GWAS-QTL colocalization events involving lncRNA genes, related to Figure 5 and Table S6

(A) The number of specific traits covered by the general trait categories used in Figure 5A and Figure S5B. The green and blue bars reflect the number of tested traits with eQTL or sQTL colocalizations (respectively) with any gene, not just lncRNA genes.

(B) Contribution of each gene type to significant colocalization events, collapsed across tissues (feature-GWAS combinations) in a separate panel for each colocalization approach. GWAS were grouped on the y axis by the general trait categories from Figure S5A. For each trait category, the top bar shows eQTL colocalizations and the bottom bar shows sQTL colocalizations. If a bar is missing from the plot, there were no colocalizations for that given trait category and QTL type. The numbers to the right of each bar are the total number of significant colocalization events.

(C) Significant lncRNA colocalization events (feature-GWAS-tissue combinations) grouped by the colocalization status of neighboring protein-coding genes. Each panel summarizes the results from one colocalization approach. Of the three colocalization approaches, SMR+HEIDI was the least favorable for finding lncRNA gene colocalizations with a strong, standalone signal, partially because this approach did not discover many lncRNA gene colocalizations to begin with. The numbers of events for each method will not sum up to the numbers in Figure 5C, since many colocalization methods were detected by multiple methods. ALS, amyotrophic lateral sclerosis; CAD, coronary artery disease; IBD, inflammatory bowel disease; UC, ulcerative colitis; MS, multiple sclerosis.